Earth-Science Reviews 226 (2022) 103918

Contents lists available at ScienceDirect

Earth-Science Reviews

journal homepage: www.elsevier.com/locate/earscirev

# From supercontinent to superplate: Late Paleozoic Pangea's inner deformation suggests it was a short-lived superplate

Daniel Pastor-Galán [a,b,*]

[a] Department of Geodynamics, University of Granada, Granada, Spain
[b] Frontier Research Institute for Interdisciplinary Science, Tohoku University, Sendai, Japan

ARTICLE INFO

*Keywords:*
Pangea
Supercontinent
Superplate
Orocline
Permian
Paleotethys
Rheic

ABSTRACT

The supercontinent cycle explains how landmasses amalgamate into supercontinents that dismember after a ~100 Myr tenure in a quasi-periodic manner. Supercontinents are thought to be rigid superplates whose formation controls many of the Earth's secular variations, from long-term climate trends to global mantle circulation. Pangea, the latest continental superplate, formed ~330 Ma, began to rift ~240 Ma, finally broke-up ~200 Ma, is generally considered the template for all previous supercontinents. The existence of Pangea as a superplate at ~330 Ma is inconsistent with: (i) the kinematic constraints of the continent-continent collision that became progressively younger westwards and it only ended in the early Permian times in its westernmost side; (ii) the widespread 'post-orogenic' magmatism in the core of Pangea and the hot high-pressure metamorphism in the Paleotethys; and (iii) the global paleomagnetic database that shows paleolatitudinal overlaps between the participating continents, and significant vertical axis rotations in the core of Pangea between 330 and 270 Ma, which suggests >1500 km of shortening and extension. Here I present a tectonic reconstruction that reconciles the paleomagnetic and geological discrepancies. In this model, after the initial amalgamation of Pangea as a landmass, the comprising plates kept on interacting between each other and the asthenosphere during the late Carboniferous and early Permian (320–270 Ma) instead of being a rigid plate. After that and concomitant with a plate reorganization, Pangea finally established as a superplate for a brief period of <70 Myr. This superplate tenure might be, following most recent models, too short to control the global mantle circulation.

## 1. Introduction

In the early 20th century, Alfred Wegener presented Pangea ('all lands' in Greek), the "primordial" continent containing all landmasses, whose break-up gave birth to our present-day Earth. Unaccepted for several decades, Pangea became a geological landmark after the discovery of seafloor spreading and advent of plate tectonics (e.g., Wilson, 1966; Ziegler, 1992). The recognition of Earth's solid outer shell as consisting of a number of rigid plates that move and interact evoking pieces of a spherical jig-saw puzzle (e.g., Vine and Matthews, 1963; McKenzie and Parker, 1967; see Moores et al., 2013 for a synthesis) revolutionized Earth sciences and made possible an understanding pre-Pangean geology under a unifying paradigm (Evans, 2013). The proposition that other unusually large continents might have existed before Pangea quickly followed and developed into the concept of the supercontinent cycle (Worsley et al., 1986; Nance et al., 1988; see Nance et al., 2014 for a historical review). The supercontinent cycle hypothesis proposes that Earth's continental plates amalgamate into single continents with a lifespan of ca. 100 Myr, which inexorably break apart, in a quasi-periodic cycle that lasts approximately 600 Myr (Nance et al., 2014; Pastor-Galán et al., 2019). The formation and disruption of supercontinents have been linked to global external changes of the Earth, for example sea-level and climate; and internal, such as large igneous provinces, deep mantle circulation or outer core dynamics (e.g., Nance et al., 1988; Mitchell et al., 2021). The external changes are mainly controlled by the size, shape, and latitude of the supercontinent mass. A significant impact on the mantle circulation likely requires supercontinents to be superplates with little interaction with the underlying mantle (Pastor-Galán et al., 2019; Heron et al., 2021).

Pangea, the most recent continental superplate (Fig. 1), has played a crucial role in the development of the supercontinent cycle hypothesis. It remains the best paleogeographically constrained supercontinent, whereas other pre-Pangean supercontinents are less understood (Evans, 2013). The kinematics of Pangea's disassembly is well understood owing

* Corresponding author at: Department of Geodynamics, University of Granada, Granada, Spain.
*E-mail address:* dpastorgalan@ugr.es.

https://doi.org/10.1016/j.earscirev.2022.103918
Received 17 February 2021; Received in revised form 2 January 2022; Accepted 3 January 2022
Available online 11 January 2022

to the preservation of the ocean floor that grew between its components (Müller et al., 2019). In contrast, the amalgamation and stability period of Pangea remains puzzling. The collision of Gondwana and Laurussia (the Variscan-Alleghanian Orogen, Devonian-Carboniferous; Fig. 2) is generally considered the inception of the supercontinent, which continued growing during the Permian in the Central Asian Orogenic Belt (CAOB) at its eastern side (Fig. 3; e.g., Safonova and Santosh, 2014; Ganbat et al., 2021). Most tectonic reconstructions assume that Pangea was a single and stable superplate from ca. 330 Ma (Domeier et al., 2012; Stampfli et al., 2013; Wu et al., 2021). However, this hypothesis of a Pangean superplate from ca. 330 Ma is not consistent with several observations:

1) The Variscan-Alleghanian continent-continent collision was diachronous and became progressively younger westwards (in present-day coordinates): from Devonian age along the eastern boundary, progressing to Early Permian ages in the westernmost sector (e.g., Hatcher, 2002; Chopin et al., 2014; Franke et al., 2017).
2) An enhanced thermal regime with widespread post-orogenic (between 310 and 270 Ma) magmatism in the core of Pangea (Pereira et al., 2014; Yuan et al., 2020) was accompanied by particularly hot high-pressure metamorphism (Tsujimori and Ernst, 2014).
3) The paleomagnetic database that shows: (a) significant vertical axis rotations that imply thousands of kilometers of shortening and/or extension (depending on the location of the Euler poles) within the supercontinent (e.g., Pastor-Galán et al., 2018). And (b) paleolatitudinal inconsistencies that suggest over 1000 km latitudinal overlaps between Gondwana and Laurussia in conventional Pangea "A" (Wegener style) reconstructions (Domeier et al., 2012; Gallo et al., 2017; Kent and Muttoni, 2020).

This resulted in a long-term debate on how the Pangean superplate formed, which geometry and continental configuration had (Pangea A vs. B debate) and which geodynamic consequences the formation of Pangea carried (Dang et al., 2020; Murphy and Nance, 2008, 2013; Stampfli et al., 2013; Yoshida and Hamano, 2015; Wang et al., 2020; Kent and Muttoni, 2020). In this paper, I present a plate reconstruction that reconciles paleomagnetic and geological data and shows that the Pangea superplate was likely shorter-lived than previously thought, despite being a long-lived, but tectonically active, supercontinent.

## 2. Methodology

### 2.1. Parent model and fundamental data

This paper reconstructs plate configurations of Pangea's interior between 320 and 270 Ma in a paleomagnetic reference frame supported by multiple geologic observations and semiquantitative data. For practical reasons, the tectonic model presented in this paper is grounded on the plate model of CEED, University of Oslo, Norway for the late Paleozoic (e.g., Domeier and Torsvik, 2014; Torsvik and Cocks, 2017). In contrast with other models (e.g., Stampfli et al., 2013), CEED's model is publicly available, open source and fully customizable. CEED's model relies upon a global paleomagnetic dataset (Torsvik et al., 2012), a catalog of large igneous provinces and kimberlite distributions and a wealth of qualitative and quantitative geologic and paleontological data (e.g., Torsvik and Cocks, 2017).

A particular feature of the CEED model is that it estimates pre-Jurassic paleolongitudes following the contested assumption (see Heron, 2019 for a synthesis on the debate) that the lowest mantle Large Low Shear wave Velocity Provinces (Niu et al., 2018; Doucet et al., 2020; Fig. 4) have remained stable from the earliest Paleozoic (Torsvik et al., 2008; Burke et al., 2008). The model uses kimberlite outcrops and large igneous provinces, which commonly occur over the margins of the LLSVPs when reconstructed to their original positions in a mantle reference frame allowing to set provisional paleolongitudes (Domeier and Torsvik, 2014). CEED reconstruction, finally, follows a mantle reference frame and is corrected for true polar wander (TPW)

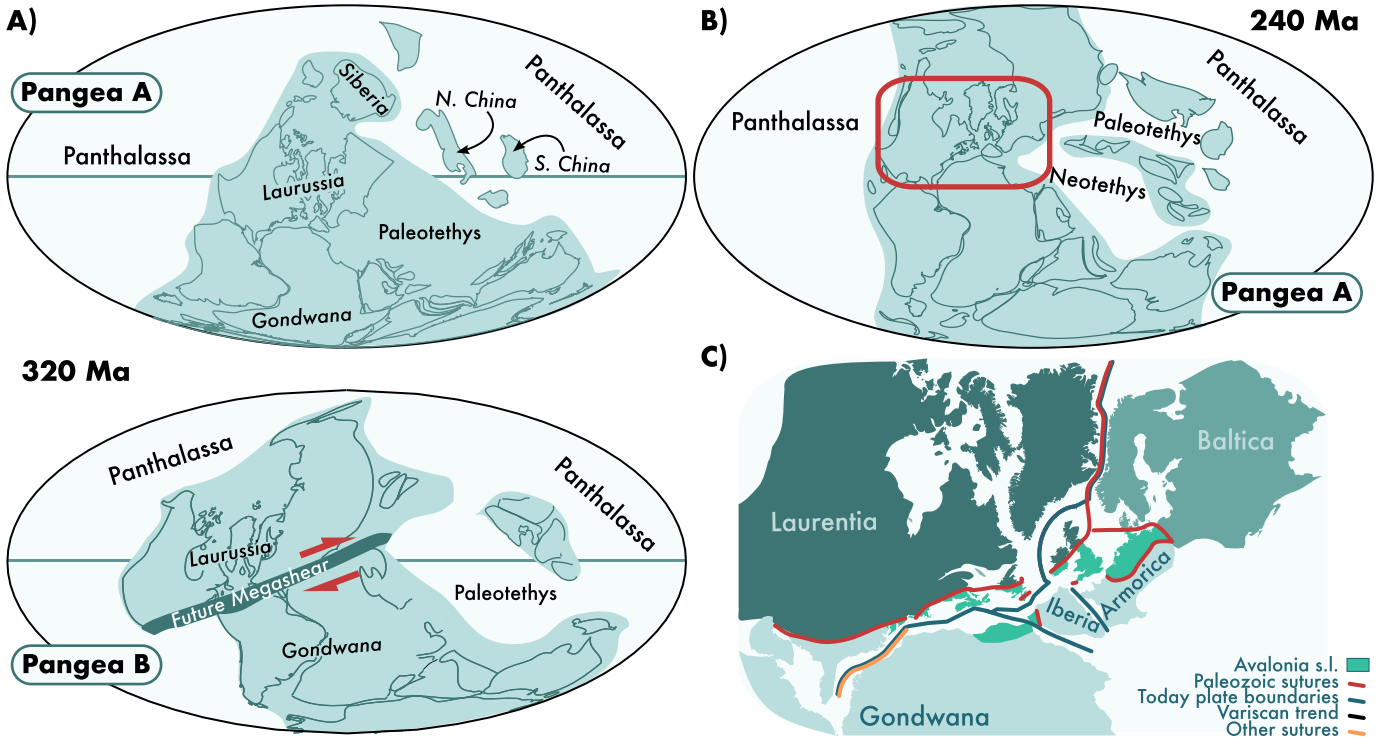


**Fig. 1.** The Two faces of Pangea A) Classic views of Pangea A and B during the late Carboniferous, with a line marking the equator and the accepted Early Triassic Pangea A. B) Distribution of the landmasses, present-day plate boundaries and oceanic sutures in the core of Pangea. Note that counterintuitively, Pangea broke too far from some pre-existing oceanic sutures and weak lithospheric zones, even cross cutting cratonic areas.

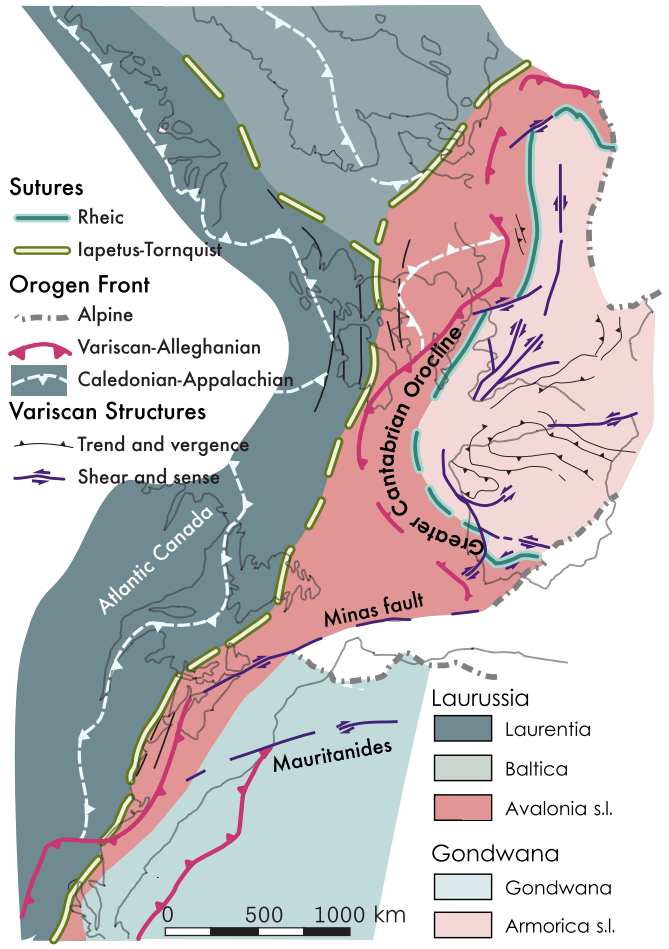


**Fig. 2.** Schematic and simplified paleogeographic map of the Variscan–Alleghanian orogeny before the breakup of Pangea. The map represents Iberian outcrops without considering post-Jurassic Alpine deformation (modified from Pastor-Galán et al., 2020).

(Steinberger and Torsvik, 2008). It is worthy to mention that this feature, although potentially useful, is not crucial for the model presented in this paper, is adaptable to other models built on paleomagnetic reference frames (e.g., Scotese et al., 2021) or mixed models such as Stampfli et al. (2013).

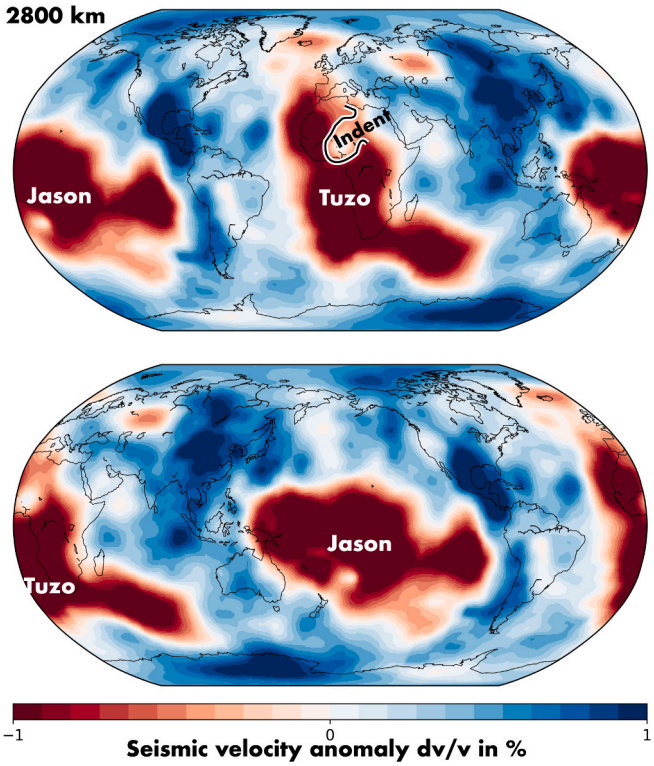


**Fig. 4.** LLSVPs at 2800 km from an average S-wave model in Submachine. Models chosen: SP12RTS-S; SPani-S; TX2019slab-S; S362ANI+M; S40RTS; TX2015; SEISGLOB1; SEISGLOB2. Hosseini et al., 2018 and Shephard et al., 2017.

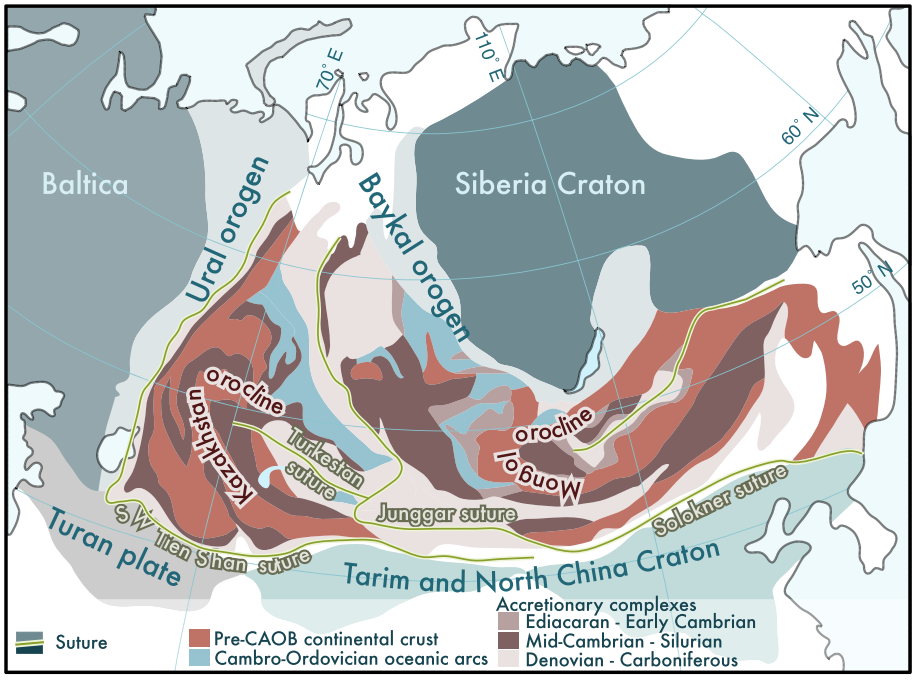


**Fig. 3.** Simplified map of the Central Asian Orogenic Belt (CAOB). The map represents the main suture zones and (modified from Xiao et al., 2015).

Paleomagnetism, which informs about paleolatitudes and vertical axis rotations of continents, can quantify past motions between continental blocks even when they are not connected to oceanic crust through a passive margin. Paleozoic paleomagnetic records are available only from continents (there is no pre-Jurassic oceanic lithosphere preserved) and their quantity and quality are highly variable in both space and time. For the reconstruction of the inner Pangean kinematics between 320 and 270 Ma, I used the most recent global compilation of paleomagnetic poles for the Phanerozoic (Torsvik et al., 2012) and a compilation of all available paleomagnetic data from the Variscan orogen (Table 1 and references therein), from Poland to Iberia and the Atlantic coast of North America, in the time from 330 and 280 Ma that met a minimum of quality pre-requirements. Robust paleomagnetic poles come from well-determined, independent readings of the geomagnetic field over a time period that is long enough to average the effect of paleosecular variation of the geomagnetic field, but short enough to not integrate appreciable plate motion. Site mean directions must be averaged properly to be transformed to virtual geomagnetic poles (VGPs) (e.g., Deenen et al., 2011). For this compilation, I have applied the following filtering criteria to site mean directions excluding sites that: (i) do not provide a stepwise demagnetization, (ii) age of magnetization is not precisely determined (±7 myr), (iii) number of samples is less than 7, (iv) concentration parameter (k) is too low (<8) or α95 values (the radius of the 95% confidence interval on the mean direction) is greater than 20°. Paleomagnetic poles, predicted inclinations, and paleolatitudes are listed in Table 1. Paleogeographically, the newly compiled data come from both Gondwana and Laurussia margins, most of them from the area putatively deformed by shearing during the Pangea B to Pangea A transition in the middle Permian. The reconstruction fulfills all paleomagnetic constraints, both from the orogenic areas (Fig. 5) and from stable Laurussia and Gondwana, including those suggesting large overlaps in classical Pangea A reconstructions (Figs. 1 and 4; Table 1).

A variety of geological data from the core of Pangea and the Paleotethyan realm were reviewed and used in the model, firstly, to test and constrain the continental movements inferred from paleomagnetic data and secondly, to communicate information about plate interactions, kinematics, dynamics and relative paleolatitudes and longitudes (see next section). Broadly, the compiled and presented geologic data include spatial-temporal details of regionally important episodes of magmatism, metamorphism and orogenesis, as well as key stratigraphic and structural relationships. They have been organized spatially, according to qualitatively defined margins, to facilitate the construction of simplified plate boundaries.

### 2.2. Building the kinematic model

The kinematic reconstruction has been performed with GPlates software (Boyden et al., 2011) to modify the CEED network of plate boundaries and Euler rotations. In addition, the model takes advantage of the capability of GPlates to reconstruct deforming plates (Gurnis et al., 2018) allowing the investigation on the effects of collision between Laurussia and Gondwana on Pangea's paleogeography. With GPlates I have modified the plate boundary network of the CEED model within the core of Pangea by drawing new polygons (Fig. 6; Table 2) from the relative motions described by the continental reconstruction based on paleomagnetic data and from the interpretation of the compiled geological data (see Section 3). For example, structural geology offers information about compression, extension, and motion along different kind of faults and plate boundaries. Likewise, observations of arc magmas, high (HP) or ultra-high (UHP) pressure metamorphic rocks, ophiolite and serpentinite mélange occurrences indicative of past convergent margins are useful for inferring the duration and sometimes even the polarity of the subduction zone. Finally, rift-related sedimentary sequences and A-type magmatism point to the development of divergent margins. Well curated paleontological data offer interesting insights into paleography, informs about relative paleolatitudes, proximity of continents, width of ocean basins, and together with paleomagnetic and other geological data may provide constraints on relative longitude.

When boundaries are unclear or unidentified, the kinematic model itself, which employs the basic plate tectonic principles, interprets the character and the location of plate boundaries within the geographic domain of the continents. In this manner, if two continents describe a relative motion that separates them, the model will predict a divergent margin, even when not documented so far in the geology. Reconstruction of a plate motion is an iterative process: boundaries must meet all geologic constraints at a given time and evolve with kinematic continuity to fit the observations and data of other times. As solutions are not unique, the best viable model considered is the simplest one that fulfills the studied constraints.

Although the plate boundaries of the Paleotethys ocean in this reconstruction have been modified from CEED's original, its connection with Panthalassa Ocean fits with the parent model, making the modifications consistent with the previous model. At the European and northwestern North American realms, the original blocks of CEED have been modified to accommodate the paleomagnetic and geological observations (see Section 4; Figs. 6 and 7, and Table 2). The plate circuit of this paper's model ends in South Africa following the proposal of Torsvik et al. (2012). However, two solutions for the movement of South Africa (Gondwana) are provided. (1) South African coordinates following the CEED model (Supplementary Datafile S2), which used the TPW corrections from CEED and fits the LLSVPs with plume volcanism and kimberlite occurrences, and therefore provides approximate paleolongitudes in a mixed paleomagnetic and mantle reference frame. This is the preferred solution. (2) South African coordinates from the Gondwana APWP of Gallo et al. (2017). This version shows the best paleomagnetic fit and forces a global net rotation whose correction would require a certain amount of TPW that has not been quantified in this paper. The latter model has a poorer fit between kimberlites and LLSVP's. From 270 Ma to 250 Ma both versions join the CEED plate model.

After constructing the polygon model, I created a deforming topological network in GPlates to visualize the intraplate deformation (Fig. 6), since rigid polygons do not properly assess the sense of continuum and preclude the interpretation of the deformation. In contrast, a deforming topological network can help to match the geological observations with the model predictions in terms of plate boundaries, shortened and extended areas and major transform faults (Fig. 8 and Fig. 9). My deforming topological network simulates a deformable sector of the Pangean supercontinent. The network consisted of one point centered in each rigid block that were deforming and rotating in the reconstructed time. I have iteratively changed the Euler rotations until both paleomagnetism and deformation described in the literature were mimicked by the deformable plate. In turn, the deformable plate predicted where data was not available the prospective locations of plate boundaries, polarity of subduction, development of basins…

## 3. Geological background, observations, and disagreements

The geometry and kinematics of Pangea just before and during its break-up are reasonably constrained. In the early Mesozoic era (ca. 240 Ma) extension commenced in Pangea between present-day NW Africa and North America (Kneller et al., 2012; Müller et al., 2019). After a 40 Myr period of extension, oceans formed in the Early Jurassic (Müller et al., 2019) and the process continued until now, with Pangea's former constituents dispersed and globally distributed (Torsvik et al., 2012). The break-up of Pangea was assisted by plume magmatism of the Central Atlantic Magmatic Province (CAMP) (Denyszyn et al., 2018). This large Igneous Province (LIP) originated above the periphery of the Large Low Shear Velocity Province (LLSVP) known as TUZO (Fig. 4; Burke, 2011; Burke et al., 2008). Pangea's amalgamation is, in contrast, far more disputed.

**Table 1**
Compilation of paleomagnetic poles used in this paper.

| Rock Fm. | Location | Mag. | I corr. | Age Mag. | | Q | A95 | Pole | | EULER (270 Ma) | GPDB RefNo/Reference | Notes |
|---|---|---|---|---|---|---|---|---|---|---|---|---|
| | | | | Published | Est. | VdV | | Lat | Lon | (Baltica coord.) | | |
| **W-Avalonia - Laurentia** | | | | | | | | | | | | |
| Minudie Point | Nova Scotia | P | | 312 | | | 6 | **36.0** | **122.0** | 78.6/161.9/31 | van der Voo, 1993 | |
| New Brunswick Volcanics I | New Brunswik | S.F. | | L.C. | 315–300 | | 10 | **21.0** | **135.0** | 78.6/161.9/31 | van der Voo et al., 1997 | |
| Pennsylvania red beds | New Brunswik | S.F. | | L.C. | 315–300 | | 3 | **42.0** | **130.9** | 78.6/161.9/31 | Miller and Kent, 1986 | |
| Shepody Fm., Nova Scotia | Nova Scotia | P | on paper | 317 | | 7 | 7.7 | **−27.2** | **298.3** | 78.6/161.9/31 | Bilardello and Kodama (2010) | |
| Mauch Chunk | Pennsylvanya | P | on paper | 320 | | 6 | 8.3 | **−22.6** | **294.4** | 78.6/161.9/31 | Bilardello and Kodama (2010) | |
| Maringouin Fm. | Nova Scotia | P | on paper | 322 | | 7 | 15.3 | **−27.9** | **297.2** | 78.6/161.9/31 | Bilardello and Kodama (2010) | |
| Volcanics & redbeds | New Brunswick | N.C. | | 330 | 320–310 | 4 | 6.5 | **−19.5** | **315.8** | 78.6/161.9/31 | K.-Seguin and Clark (1985) | Single polarity (Kiaman) |
| Jeffreys Village Member | New Foundland | P | | 333 | | 6 | 8 | **−27.0** | **311.0** | 78.6/161.9/31 | 1534, T | Single polarity (Kiaman) |
| Deer Lake Fm. | New Foundland | P | on paper | 335 | | 7 | 9 | **−18.6** | **304.2** | 78.6/161.9/31 | Bilardello and Kodama (2010) | Single polarity (Kiaman) |
| Catskill Fm. South | Pennsylvanya | N.C. | | 370 | 320–310 | 3 | 16 | **−27.4** | **303.0** | 78.6/161.9/31 | Miller and Kent, 1986 | Single polarity (Kiaman) |
| **Laurussia-North UK** | | | | | | | | **Poles plotted together with the Variscan in Supplementary File 1** | | | | |
| ORS-Glenn-Scotland | Scotland | P.F.C. | | E.P. | 300–280 | | 18.8 | **28.9** | **179.0** | | Elmore et al., 2006 | |
| ORS-Glenn-Scotland, PRE | Scotland | P.F.C. | | L.C. | 310–295 | | 7.3 | **−24.4** | **−32.1** | | Elmore et al., 2006 | |
| ORS Scotland | Scotland | P.F.C. | | L.C. | 310–295 | | 2.7 | **29.9** | **170.2** | | Storetvedt et al., 1990 | |
| ORS Scotland | Scotland | P.F.C. | | L.C. | 310–295 | | 5.7 | **26.7** | **144.3** | | Storetvedt et al., 1990 | Compilation, references therein |
| Pre-Devonian Dol | Scotland | P.F.C. | | E.P. | 300–280 | | 7.5 | **38.7** | **173.6** | | Elmore et al., 2000 | |
| Pre-Devonian Dol | Scotland | P.F.C. | | E.P. | 300–280 | | 16.9 | **41.7** | **165.8** | | Elmore et al., 2000 | |
| Clare Island | Ireland | P.F.C. | | L.C.- E.P. | 305–295 | | 5 | **−36.6** | **−29.7** | | Smethurst and Briden, 1988 | Recalculated from original data |
| Mauchline lavas, Scotland | Scotland | P | | 280 | | 3 | 14 | **−47.0** | **337.0** | | 3093, T | From Torsvik et al., 2012 |
| Peterhead dyke | Scotland | P | | 297 | | 5 | 1.3 | **−41.0** | **342.0** | | 1535, T | From Torsvik et al., 2012 |
| Queensferry sill | Scotland | P | | 305 | | 5 | 5.2 | **−38.3** | **354.0** | | 2447, T | From Torsvik et al., 2012 |
| Salrock | Ireland | P.F.C. | | L.C.- E.P. | 305–295 | | 4 | **−31.0** | **−28.9** | | Smethurst and Briden, 1988 | |
| Salrock | Ireland | P.F.C. | | L.C.- E.P. | 305–295 | | 9.3 | **−38.6** | **−25.4** | | Smethurst et al., 1994 | |
| **E-Avalonia** | | | | | | | | | | | | |
| Salrock | Ireland | P.F.C. | | E.P. | 300–280 | | | **−47.6** | **−14.5** | | Smethurst et al., 1994 | |
| ORS Wales-Area 3 | Wales | | | L.C.- E.P. | 305–295 | | 1.9 | **−41.2** | **341.1** | | Setiabudidaya et al., 1994 | |

(*continued on next page*)

**Table 1** (*continued*)

| Rock Fm. | Location | Mag. | I corr. | Age Mag. | | Q | A95 | Pole | | EULER (270 Ma) | GPDB RefNo/Reference | Notes |
|---|---|---|---|---|---|---|---|---|---|---|---|---|
| | | | | Published | Est. | VdV | | Lat | Lon | (Baltica coord.) | | |
| | | P.F. | | | | | | | | | | |
| | | C. | | | | | | | | | | |
| | | P.F. | | | | | | | | | | |
| ORS Wales-Group 2 | Wales | C. | | L.C.- E.P. | 305–295 | | 1.6 | **−36.6** | **327.0** | | Setiabudidaya et al., 1994 | |
| ORS Wales | Wales | S.F. | | L.C. | 315–300 | | 6.1 | **−29.7** | **−44.6** | | Setiabudidaya et al., 1994 | |
| ORS Wales | Wales | S.F. | | L.C. | 315–300 | | 11.6 | **−28.4** | **−62.8** | | Setiabudidaya et al., 1994 | |
| Mendips volcanics | S England | | | L.C.- E.P. | 310–295 | | 5.4 | **25.0** | **339.0** | | Torsvik et al., 1993 | |
| Craven | N England | | | L.C.- E.P. | 300–290 | | 4.7 | **−39.4** | **346.0** | | McCabe and Channell, 1994 | |
| Exeter Lavas | S England | | | 280 | 285–275 | | 19 | **−46.0** | **345.0** | | Mac Niocaill, 2000 | Compilation, references therein |
| Whin Sill | N England | | | 281 | 285–275 | | 5 | **−44.0** | **339.0** | | Mac Niocaill, 2000 | Compilation, references therein |
| Wackerfield Dyke | N England | | | L.C.- E.P. | 300–290 | | 3 | **−49.0** | **349.0** | | Mac Niocaill, 2000 | Compilation, references therein |
| Hendre/Blodwell intrusives | N England | | | L.C.- E.P. | 300–290 | | 12 | **−32.0** | **337.0** | | Mac Niocaill, 2000 | Compilation, references therein |
| Bristol ORS | England | RM | | E.P. | 300–280 | | 9 | **−32.0** | **338.0** | | Mac Niocaill, 2000 | Compilation, references therein |
| Peel sandstone (comp.) | Isle of Man | P.F.<br>C. | | L.C. | 320–300 | | 3.8 | **148.2** | **50.3** | | Piper and Crowley, 1999 | |
| DINGLE Recalculated | Ireland | P.F.<br>C. | | L.C.- E.P. | 305–295 | | 4.2 | **−34.0** | **−31.5** | | Storetvedt et al., 1993 | |
| Mill Cove Red beds I componet | Ireland | P.F.<br>C. | | L.C. | 310–295 | | 10.8 | **−43.0** | **330.0** | | Mac Niocaill, 2000 | |
| Munster Basin | Ireland | P.F.<br>C. | | 314–290 | | | 2.6 | **31.0** | **132.5** | | (Pastor-Galán et al., 2015b) | |
| Holy Island Sill & Dyke (Whin Sill) | N England | P | | 294 | | 5 | 6.3 | **−35.4** | **346.8** | | T, Liss et al. (2004) | From Torsvik et al., 2012 |
| Alnwick Sill, (Whin Sill) | N England | P | | 294 | | 5 | 8.1 | **−47.1** | **337.1** | | T, Liss et al. (2004) | From Torsvik et al., 2012 |
| Devonian Limestone – B | Ardenn-Rotated Limb | S.F. | | L.C. | 310–305 | | 3.1 | **−27.7** | **−42.8** | | Zegers et al., 2003 | Recalculated from original data |
| Devonian Limestone – B | Ardenn-Less R Limb | S.F. | | L.C. | 310–305 | | 3 | **−31.5** | **−23.4** | | Zegers et al., 2003 | Recalculated from original data |
| Devonian Limestone – B | Ardennes A | P.F.<br>C. | | E.P. | 300–280 | | 1.4 | **−37.9** | **−26.0** | | Zegers et al., 2003 | Recalculated from original data |
| Igneous – B | Bohemian Massif | RM | | 325–320 | | 4 | 2.8 | **−5.6** | **−53.3** | | Edel, 2003 | Recalculated from original data |
| Devonian Limestone | Bohemian Massif | P.F.<br>C. | | L.C. | 305–295 | 3 | 16.3 | **−35.2** | **−12.3** | | Tait et al., 1997 | |
| Metamorphics | Bohemian Massif | RM | | 315 | 320–310 | | 13 | **−6.0** | **319.0** | | Edel et al., 2018 | Compilation, references therein |
| Metamorphics | Bohemian Massif | RM | | 315 | 320–310 | | 17.5 | **17.0** | **322.0** | | Edel et al., 2018 | Compilation, references therein |
| Metamorphics | Bohemian Massif | RM | | 315 | 320–310 | | 21 | **−2.0** | **319.0** | | Edel et al., 2018 | Compilation, references therein |
| Metamorphics | Bohemian Massif | RM | | 315 | 320–310 | | 14.6 | **−4.0** | **318.0** | | Edel et al., 2018 | Compilation, references therein |
| Metamorphics | Bohemian Massif | RM | | 308 | 310–305 | | 7.8 | **−26.0** | **334.0** | | Jeleńska et al., 2003 | |
| Devono-Carb (I comp) | Bohemian Massif | P.F.<br>C. | | 320 | | | 5.5 | **−26.0** | **327.0** | | Nawrocki, 1993 | |
| Devono-Carb (A comp) | Bohemian Massif | | | 290 | | | 2.5 | **−42.0** | **342.0** | | Nawrocki, 1993 | |

(*continued on next page*)

**Table 1** (*continued*)

| Rock Fm. | Location | Mag. | I corr. | Age Mag. | | Q | A95 | Pole | | EULER (270 Ma) | GPDB RefNo/Reference | Notes |
|---|---|---|---|---|---|---|---|---|---|---|---|---|
| | | | | Published | Est. | VdV | | Lat | Lon | (Baltica coord.) | | |
| Devono-Carb (B comp) | Bohemian Massif | P.F. C. P.F. C. | | 315 | | | 9.1 | **−10.0** | **304.0** | | Nawrocki, 1993 | |
| Quartz porphyry, Germany | Bohemian Massif | P | | 280 | | 4 | 7 | **−37.0** | **341.0** | | 3145, T | From Torsvik et al., 2012 |
| Igneous, Germany | Bohemian Massif | P | | 280 | | 5 | 10 | **−42.0** | **346.0** | | 2356, T | From Torsvik et al., 2012 |
| Intrasudetic Basin volcanics | Bohemian Massif | P | | 285 | | 5 | 3.2 | **−43.0** | **352.0** | | 3161, T | From Torsvik et al., 2012 |
| North Sudetic Basin, Poland | Bohemian Massif | P | | 285 | | 5 | 5.1 | **−44.0** | **4.0** | | 3161, T | From Torsvik et al., 2012 |
| Krkonose Basin, Czech Republic | Bohemian Massif | P | | 285 | | 5 | 2 | **−40.0** | **346.0** | | 2444, T | From Torsvik et al., 2012 |
| North Sudetic Basin volcanics | Bohemian Massif | P | | 285 | | 4 | 8.1 | **−42.0** | **354.0** | | 3161, T | From Torsvik et al., 2012 |
| Intrasudetic basin sediments | Bohemian Massif | P | | 285 | | 4 | 6.8 | **−37.0** | **340.0** | | 3161, T | From Torsvik et al., 2012 |
| Krakow volcanics, Poland | Bohemian Massif | P | | 285 | | 4 | 7.9 | **−43.0** | **345.0** | | 275, T | From Torsvik et al., 2012 |
| Red beds, Czech Republic | Bohemian Massif | P | | 285 | | 5 | 4 | **−41.0** | **345.0** | | 167, T | From Torsvik et al., 2012 |
| Lower Silesia volcanics, Poland | Bohemian Massif | P | | 285 | | 3 | 13.2 | **−40.0** | **352.0** | | 465, T | From Torsvik et al., 2012 |
| Black Forest volcanics, Germany | Bohemian Massif | P | | 286 | | 4 | 5.9 | **−49.0** | **356.0** | | 170, T | From Torsvik et al., 2012 |
| Sudetic Mountain granitoids | Bohemian Massif | P | | 293 | | 6 | 13 | **−42.0** | **346.0** | | 2446, T | From Torsvik et al., 2012 |
| Cracow volcanics A, Poland | Bohemian Massif | P | | 294 | | 4 | 4.8 | **−44.0** | **355.0** | | Nawrocki et al. (2008) | From Torsvik et al., 2012 |
| Westphalian–Stephanian red beds | Bohemian Massif | P | | 305 | | 5 | 9 | **−38.0** | **343.0** | | 167, T | From Torsvik et al., 2012 |
| Silesia volcanics, Poland | Bohemian Massif | P | | 296 | | 4 | 13.6 | **−43.0** | **354.0** | | 465, T | From Torsvik et al., 2012 |
| **Armorican-Gondwana** | | | | | | | | | | | | |
| Different Volcanics (A) | France | P | | 325 | | 4 | 1.9 | **−8.8** | **−57.5** | | Edel, 2001 | Recalculated from original data |
| Different Volcanics (B) | France | RM | | L.C.- E.P. | 305–295 | | 6.5 | **−27.1** | **−33.8** | | Edel, 2001 | Recalculated from original data |
| Different Volcanics and Red Beds | Corsica & N Sardinia | P | | 320–250 | | | 6.8 | **36.3** | **70.4** | 44.6/4.6/ −79.8 | Bachtadse et al., 2018 | Compilation, references therein |
| Different Volcanics and Red Beds | Corsica & N Sardinia | P | | 320–250 | | | 7.3 | **31.2** | **68.4** | 44.6/4.6/ −79.8 | Bachtadse et al., 2018 | Compilation, references therein |
| Different Volcanics and Red Beds | Corsica & N Sardinia | P | | Permian | 275 | | 11.5 | **38.0** | **59.0** | 44.6/4.6/ −79.8 | Bachtadse et al., 2018 | Compilation, references therein |
| Different Volcanics and Red Beds | Corsica & N Sardinia | P | | Permian | 275 | | 27 | **37.0** | **58.0** | 44.6/4.6/ −79.8 | Bachtadse et al., 2018 | Compilation, references therein |
| Different Volcanics and Red Beds | Corsica & N Sardinia | P | | 270 | | | 15 | **31.5** | **67.9** | 44.6/4.6/ −79.8 | Bachtadse et al., 2018 | Compilation, references therein |
| Different Volcanics and Red Beds | Corsica & N Sardinia | P | | 285 | | | 14 | **38.0** | **71.4** | 44.6/4.6/ −79.8 | Bachtadse et al., 2018 | Compilation, references therein |
| | S Sardinia | P | | 290 | | | 5.5 | **1.3** | **−75.6** | | Bachtadse et al., 2018 | |

(*continued on next page*)

**Table 1** (*continued*)

| Rock Fm. | Location | Mag. | I corr. | Age Mag. | | Q | A95 | Pole | | EULER (270 Ma) | GPDB RefNo/Reference | Notes |
|---|---|---|---|---|---|---|---|---|---|---|---|---|
| | | | | Published | Est. | VdV | | Lat | Lon | (Baltica coord.) | | |
| Different Volcanics and Red Beds | | | | | | | | | | 44.6/4.6/ −79.8 | | Compilation, references therein |
| Different Volcanics and Red Beds | S Sardinia | P | | 294 | | | 13.6 | **3.0** | **100.1** | 44.6/4.6/ −79.8 | Bachtadse et al., 2018 | Compilation, references therein |
| Different Volcanics and Red Beds | S Sardinia | P | | 294 | | | 9.7 | **9.3** | **−78.0** | 44.6/4.6/ −79.8 | Bachtadse et al., 2018 | Compilation, references therein |
| Dykes (Edel's A Component) | Pyrenees | P | | 280 | 305–280 | | 6.5 | **−47.3** | **321.2** | 43.9/4.29/ −30.6 | Edel et al., 2015 | Recalculated from original data |
| Dykes (Edel's B component) | Pyrenees | P | | 300 | 310–300 | | 6.9 | **−27.9** | **299.0** | 43.9/4.29/ −30.6 | Edel et al., 2015 | Recalculated from original data |
| Dykes (Edel's C Component) | Pyrenees | P | | 320 | 320–310 | | 4.3 | **−10.3** | **288.8** | 43.9/4.29/ −30.6 | Edel et al., 2015 | Recalculated from original data |
| Limestones (Vega de los Viejos) | Iberia | RM | | 310 | 315–300 | | 3.5 | **−41.8** | **58.8** | 43.9/4.29/ −30.6 | Weil et al., 2000, Weil et al., 2001, Weil et al., 2013 | Recalculated from original data |
| Limestones (La Cueta) | Iberia | RM | | 310 | 315–300 | | 4.3 | **−43.2** | **30.0** | 43.9/4.29/ −30.6 | Weil et al., 2000, Weil et al., 2001, Weil et al., 2013 | Recalculated from original data |
| Limestones (Bodón) | Iberia | RM | | 310 | 315–300 | | 4.1 | **−13.7** | **84.8** | 43.9/4.29/ −30.6 | Weil et al., 2000, Weil et al., 2001, Weil et al., 2013 | Recalculated from original data |
| Volcanics (Almadén, R2) | Iberia | RM | | 315 | | | 4.5 | **−24.0** | **280.0** | 43.9/4.29/ −30.6 | Leite Mendes et al., 2021 | |
| Volcanics (Almadén, R1) | Iberia | RM | | L.C. | 315–300 | | 4.5 | **−36.7** | **52.6** | 43.9/4.29/ −30.6 | Leite Mendes et al., 2021 | Compilation, references therein |
| Limestones (Los Navalucillos) | Iberia | RM | | 305 | 305–295 | | 5.5 | **48.2** | **223.5** | 43.9/4.29/ −30.6 | Pastor-Galán et al., 2015a | |
| Limestones (Iberian Range) | Iberia | RM | | 318 | | | 6.1 | **−7.5** | **267.2** | 43.9/4.29/ −30.6 | Pastor-Galán et al., 2018 | |
| Granites (Tormes Dome) C-comp | Iberia | P | | 318.0 | | | 3.2 | **−11.7** | **264.0** | 43.9/4.29/ −30.6 | Pastor-Galán et al., 2016 | |
| Granites-Limestones (Movavg1) | Iberia | RM | | 297.5 | | | 2.3 | **37.5** | **215.1** | 43.9/4.29/ −30.6 | Pastor-Galán et al., 2016 | |
| Granites-Limestones (Movavg2) | Iberia | RM | | 300.0 | | | 1.7 | **29.8** | **231.0** | 43.9/4.29/ −30.6 | Pastor-Galán et al., 2016 | |
| Granites-Limestones (Movavg3) | Iberia | RM | | 305.0 | | | 1.3 | **21.7** | **239.6** | 43.9/4.29/ −30.6 | Pastor-Galán et al., 2016 | |
| Granites-Limestones (Movavg4) | Iberia | RM | | 307.5 | | | 2.3 | **9.5** | **249.0** | 43.9/4.29/ −30.6 | Pastor-Galán et al., 2016 | |
| Permian (dykes & red beds) | Iberia | P | | E.P. | 300–280 | | 5.4 | **43.9** | **203.3** | 43.9/4.29/ −30.6 | Weil et al., 2010 | Avg. Pole |
| Villaviciosa | Iberia | P | | E.P. | 300–280 | | 8 | **52.0** | **200.0** | 43.9/4.29/ −30.6 | Weil et al., 2010 | Compilation, references therein |
| Rillo de Gallo (Iberia range) | Iberia | P | | E.P. | 300–280 | | 9 | **49.0** | **193.0** | 43.9/4.29/ −30.6 | Weil et al., 2010 | Compilation, references therein |
| Atienza | Iberia | P | | E.P. | 300–280 | | 2.6 | **49.6** | **204.6** | 43.9/4.29/ −30.6 | Weil et al., 2010 | Compilation, references therein |
| Atienza (andesites) | Iberia | P | | E.P. | 300–280 | | 14 | **42.0** | **208.0** | 43.9/4.29/ −30.6 | Weil et al., 2010 | Compilation, references therein |
| Atienza (andesites) | Iberia | P | | E.P. | 300–280 | | 12 | **36.0** | **203.0** | 43.9/4.29/ −30.6 | Weil et al., 2010 | Compilation, references therein |
| Viar intrusons | Iberia | P | | E.P. | 300–280 | | 6 | **43.0** | **211.0** | 43.9/4.29/ −30.6 | Weil et al., 2010 | Compilation, references therein |
| Bucaco (N Portugal) | Iberia | P | | E.P. | 300–280 | | 7 | **36.0** | **211.0** | 43.9/4.29/ −30.6 | Weil et al., 2010 | Compilation, references therein |

(*continued on next page*)

**Table 1** (*continued*)

| Rock Fm. | Location | Mag. | I corr. | Age Mag. | | Q | A95 | Pole | | EULER (270 Ma) | GPDB RefNo/Reference | Notes |
|---|---|---|---|---|---|---|---|---|---|---|---|---|
| | | | | Published | Est. | VdV | | Lat | Lon | (Baltica coord.) | | |
| Bucaco (N Portugal) | Iberia | P | | E.P. | 300–280 | | 8.6 | **41.9** | **194.2** | 43.9/4.29/−30.6 | Weil et al., 2010 | Compilation, references therein |
| Sotres Fm. (Picos de Europa) | Iberia | P | | E.P. | 300–280 | | 6.7 | **41.3** | **222.5** | 43.9/4.29/−30.6 | Weil et al., 2010 | |
| Viar basin (red beds & volcanics) | Iberia | P | | E.P. | 300–280 | | 13.1 | **51.8** | **199.2** | 43.9/4.29/−30.6 | Weil et al., 2010 | |
| Lodeve Basin | France | P | | 285 | | 5 | 2 | **−42.0** | **349.0** | | 1813, T | From Torsvik et al., 2012 |
| Lodeve B Component | France | P | | 285 | | 4 | 17 | **−49.0** | **342.0** | | 2454, T | From Torsvik et al., 2012 |
| Moissey volcanics | France | P | | 285 | | 4 | 6.7 | **−41.0** | **352.0** | | 1205, T | From Torsvik et al., 2012 |
| Black Forest rhyolites | Germany | P | | 286 | | 3 | 1 | **−42.0** | **353.0** | | 2941, T | From Torsvik et al., 2012 |
| Thuringer Forest sediments | Germany | P | | 287 | | 4 | 5.8 | **−41.5** | **340.0** | | 1792, T | From Torsvik et al., 2012 |
| Saar–Nahe volcanics | Germany | P | | 291 | | 3 | 15.9 | **−41.0** | **349.0** | | 712, T | From Torsvik et al., 2012 |
| Nahe volcanics | Germany | P | | 291 | | 3 | 13 | **−46.0** | **347.0** | | 940, T | From Torsvik et al., 2012 |
| Thuringer Forest volcanics | Germany | P | | 295 | | 4 | 7.1 | **−37.1** | **350.0** | | 1792, T | From Torsvik et al., 2012 |
| Nideck–Donon volcanics | France | P | | 294 | | 4 | 4 | **−47.0** | **348.0** | | 1010, T | From Torsvik et al., 2012 |
| Lower Nideck volcanics | France | P | | 294 | | 3 | 19 | **−42.0** | **348.0** | | 174, T | From Torsvik et al., 2012 |
| **Gondwana** | | | | | | | | ***Gondwana poles in NW Africa coordinates** | | | | |
| Gerrigong Volcanics | Australia | P | | 265 | | | 8.5 | **49.5** | **257.4** | 46.79/3.2/−56.01 | Belica et al., 2017 | From Kent and Muttoni, 2020 |
| Karoo red Beds | South Africa | P | E/Icorr | 266.5 | | | 8.5 | **49.3** | **239.4** | 46.79/3.2/−56.02 | Lanci et al., 2013 | From Kent and Muttoni, 2020 |
| Tambillos | Argentina | P | uncorr. | 267 | | | 6.5 | **49.3** | **239.4** | 46.79/3.2/−56.03 | Rapalini and Vilas, 1991 | From Kent and Muttoni, 2020 |
| Taztot Trachyandesite | Morocco | P | | 273 | | | 4.6 | **38.7** | **236.8** | 46.79/3.2/−56.04 | Daly and Pozzi, 1976 | From Kent and Muttoni, 2020 |
| Adria average | Italy | P | | 280 | | | 5.9 | **42.7** | **242.1** | 46.79/3.2/−56.05 | Kent and Muttoni, 2020 | |
| Carboniferous-Permian basins | Morocco | P | | 300–275 | | | 6.8 | **−41.4** | **52.1** | 46.79/3.2/−56.05 | Domeier et al., 2021 | Pre or synfolding |
| Carboniferous-Permian basins | Morocco | P | | 300–275 | | | 6.4 | **−41.2** | **51.1** | 46.79/3.2/−56.05 | Domeier et al., 2021 | Pre or synfolding |
| Mechra and Chougrane | Morocco | P | | 295 | | | 20.9 | **36.0** | **238.0** | 46.79/3.2/−56.06 | Wesphal et al., 1979 | From Kent and Muttoni, 2020 |
| La Colina Basalt | Argentina | P | | 300 | | | 5 | **34.4** | **235.5** | 46.79/3.2/−56.07 | Thompson and Mitchell, 1972 | From Kent and Muttoni, 2020 |
| La Tabla Fm. | Chile | P | | 310 | | | 9.6 | **21.5** | **226.8** | 46.79/3.2/−56.08 | Jesinkey et al., 1987 | From Kent and Muttoni, 2020 |
| The | Chile | P | | 310 | | | 5.7 | **26.0** | **231.5** | 46.79/3.2/−56.09 | Jesinkey et al., 1987 | From Kent and Muttoni, 2020 |
| **Gondwana (**Gallo et al., 2017**)** | | | | | | | | ***Gondwana (Gallo et al.) poles in S Africa coordinates** | | | | |

(*continued on next page*)

**Table 1** (*continued*)

| Rock Fm. | Location | Mag. | I corr. | Age Mag. | | Q | A95 | Pole | | EULER (270 Ma) | GPDB RefNo/Reference | Notes |
|---|---|---|---|---|---|---|---|---|---|---|---|---|
| | | | | Published | Est. | VdV | | Lat | Lon | (Baltica coord.) | | |
| True Dipole Pole | | Avg. | | 370–330 | | | 5.1 | **−12.5** | **17.5** | 46.04/3.89/−58.2 | Gallo et al., 2017 | |
| Wester Gondwana Mean | | Avg. | | 370–330 | | | 10.5 | **−21.2** | **26.0** | 46.04/3.89/−58.2 | Gallo et al., 2017 | |
| Eastern Gondwana Mean | | Avg. | | 370–330 | | | 7.7 | **−10.5** | **10.7** | 46.04/3.89/−58.2 | Gallo et al., 2017 | |
| Mean (GAD formula) | | Avg. | | 370–330 | | | 8.7 | **−15.2** | **17.1** | 46.04/3.89/−58.2 | Gallo et al., 2017 | |
| True Dipole Pole | | Avg. | | 320–300 | | | 7.9 | **−29.5** | **60.4** | 46.04/3.89/−58.2 | Gallo et al., 2017 | |
| Wester Gondwana Mean | | Avg. | | 320–300 | | | 3.4 | **−30.2** | **57.7** | 46.04/3.89/−58.2 | Gallo et al., 2017 | |
| Eastern Gondwana Mean | | Avg. | | 320–300 | | | 9 | **−23.2** | **57.2** | 46.04/3.89/−58.2 | Gallo et al., 2017 | |
| Mean (GAD formula) | | Avg. | | 320–300 | | | 3.2 | **−28.7** | **57.6** | 46.04/3.89/−58.2 | Gallo et al., 2017 | |
| True Dipole Pole | | Avg. | | 290–270 | | | 3.6 | **−33.2** | **63.3** | 46.04/3.89/−58.2 | Gallo et al., 2017 | |
| Wester Gondwana Mean | | Avg. | | 290–270 | | | 6.5 | **−32.1** | **71.7** | 46.04/3.89/−58.2 | Gallo et al., 2017 | |
| Eastern Gondwana Mean | | Avg. | | 290–270 | | | 8.3 | **−33.2** | **73.6** | 46.04/3.89/−58.2 | Gallo et al., 2017 | |
| Mean (GAD formula) | | Avg. | | 290–270 | | | 4.5 | **−32.5** | **72.4** | 46.04/3.89/−58.2 | Gallo et al., 2017 | |
| **Laurentia** | | | | | | | | | | | | |
| Intrusions Southern Illinois | North America | P | | 270 | | 5 | 3.8 | **−56.3** | **302.9** | 78.6/161.9/31 | Domeier et al., 2011a | From Torsvik et al., 2012 |
| Downey Bluff sill | North America | P | | 272 | | 4 | 3.8 | **−53.0** | **308.7** | 78.6/161.9/31 | Reynolds et al. (1997) | From Torsvik et al., 2012 |
| Hicks Dome breccia | North America | P | | 272 | | 4 | 8.6 | **−54.8** | **292.1** | 78.6/161.9/31 | Reynolds et al. (1997) | From Torsvik et al., 2012 |
| Toroweap Formation | North America | P | | 277 | | 3 | 10 | **−56.5** | **311.0** | 78.6/161.9/31 | 688, T | From Torsvik et al., 2012 |
| Leonardian subset | North America | P | | 277 | | 3 | 5 | **−53.7** | **304.0** | 78.6/161.9/31 | 688, T | From Torsvik et al., 2012 |
| Artinskian Pictou red beds | North America | P | | 280 | | 7 | 3.6 | **−41.4** | **306.4** | 78.6/161.9/31 | 2281, T | From Torsvik et al., 2012 |
| Churchland pluton | North America | P | | 282 | | 5 | 16.3 | **−33.5** | **306.3** | 78.6/161.9/31 | 1264, T | From Torsvik et al., 2012 |
| Fountain & Lykins Fm.s | North America | P | on paper | 283 | | 4 | 13.1 | **−44.6** | **305.3** | 78.6/161.9/31 | 504 | From Torsvik et al., 2012 |
| Abo Fm. | North America | P | on paper | 285 | | 5 | 2.1 | **−46.8** | **304.0** | 78.6/161.9/31 | 1311, T | From Torsvik et al., 2012 |
| Piedmont Mafic intrusions | North America | P | | 289 | | 3 | 10.2 | **−38.9** | **300.8** | 78.6/161.9/31 | 1527 | From Torsvik et al., 2012 |
| Upper Casper Fm. | North America | P | | 291 | | 5 | 1.5 | **−50.5** | **303.0** | 78.6/161.9/31 | 1455, T | From Torsvik et al., 2012 |
| Elephant Canyon Fm. | North America | P | on paper | 292 | | 4 | 5 | **−37.5** | **296.6** | 78.6/161.9/31 | 671, T | From Torsvik et al., 2012 |
| Cutler Fm., Lisbon Valley | North America | P | on paper | 292 | | 5 | 7.1 | **−40.1** | **307.7** | 78.6/161.9/31 | 1341, T | From Torsvik et al., 2012 |
| Ingelside Fm. | North America | P | | 292 | | 5 | 2 | **−43.1** | **307.9** | | 1142, T | |

(*continued on next page*)

**Table 1** (*continued*)

| Rock Fm. | Location | Mag. | I corr. | Age Mag. | | Q | A95 | Pole | | EULER (270 Ma) | GPDB RefNo/Reference | Notes |
|---|---|---|---|---|---|---|---|---|---|---|---|---|
| | | | | Published | Est. | VdV | | Lat | Lon | (Baltica coord.) | | |
| | | | on paper | | | | | | | 78.6/161.9/31 | | From Torsvik et al., 2012 |
| Cutler Fm. | North America | P | on paper | 292 | | 4 | 2 | **−41.6** | **300.4** | 78.6/161.9/31 | 671, T | From Torsvik et al., 2012 |
| Minturn & Maroon Fm.s | North America | P | on paper | 298 | | 4 | 2.8 | **−40.1** | **300.5** | 78.6/161.9/31 | 1685, T | From Torsvik et al., 2012 |
| Upper Maroon Fm. | North America | P | on paper | 299 | | 4 | 12.8 | **−55.3** | **279.8** | 78.6/161.9/31 | 504, T | From Torsvik et al., 2012 |
| Dunkard Fm. | North America | P | | 300 | | 5 | 3.9 | **−44.1** | **301.5** | 78.6/161.9/31 | 302, T | From Torsvik et al., 2012 |
| Laborcita Fm. | North America | P | | 301 | | 5 | 2.1 | **−42.1** | **312.1** | 78.6/161.9/31 | 1311, T | From Torsvik et al., 2012 |
| Wescogame Fm. | North America | P | on paper | 301 | | 5 | 3.4 | **−44.1** | **303.9** | 78.6/161.9/31 | 1311, T | From Torsvik et al., 2012 |
| Glenshaw Fm. | North America | P | on paper | 303 | | 6 | 3.1 | **−28.6** | **299.9** | 78.6/161.9/31 | Kodama (2009) | From Torsvik et al., 2012 |
| Lower Casper Fm. | North America | P | | 303 | | 5 | 1.8 | **−45.7** | **308.6** | 78.6/161.9/31 | 1455, T | From Torsvik et al., 2012 |
| Riversdale Group | North America | P | | 310 | | 5 | 6 | **−36.0** | **302.0** | 78.6/161.9/31 | 1110, T | From Torsvik et al., 2012 |
| Peterhead dyke | Scotland | P | | 297 | | 5 | 1.3 | **−41.0** | **342.0** | | 1535, T | From Torsvik et al., 2012 |
| Queensferry sill | Scotland | P | | 305 | | 5 | 5.2 | **−38.3** | **354.0** | | 2447, T | From Torsvik et al., 2012 |
| **Baltica - And stable Europe (post 270 Ma)** | | | | | | | | | | | | |
| Esterel extrusives, France | France | P | | 264 | | 5 | 6.1 | **−51.5** | **322.0** | | 165, T | From Torsvik et al., 2012 |
| Cracow volcanics B | Poland | P | | 269 | | 4 | 4.1 | **−50.0** | **344.0** | | Nawrocki et al. (2008) | From Torsvik et al., 2012 |
| Lunner dikes, Norway | Norway | P | | 271 | | 5 | 2.5 | **−51.0** | **343.0** | | Dominguez et al. (2011) | From Torsvik et al., 2012 |
| Lunner dikes, Norway | Norway | P | | 271 | | 5 | 5.9 | **−53.0** | **344.0** | | 3188, T (redated) | From Torsvik et al., 2012 |
| Bohuslan dikes combined, Sweden | Sweden | P | | 275 | | 4 | 8.6 | **−51.0** | **345.0** | | 1155, T | From Torsvik et al., 2012 |
| Scania melaphyre dikes, Sweden | Sweden | P | | 279 | | 4 | 11 | **−54.0** | **352.0** | | 2222, T | From Torsvik et al., 2012 |
| Oslo volcanics | Norway | P | | 281 | | 5 | 1 | **−47.0** | **337.0** | | 915, T | From Torsvik et al., 2012 |
| Ringerike lavas | Norway | P | | 281 | | 4 | 13.4 | **−44.6** | **337.4** | | 1830 | From Torsvik et al., 2012 |
| Sarna alkaline intrusion | Sweden | P | | 281 | | 4 | 6.9 | **−38.0** | **346.0** | | 1735, T | From Torsvik et al., 2012 |
| Trachytes | Ukraine | P | | 282.6 | | 5 | 6.5 | **−49.4** | **359.7** | | Yuan et al. (2011) | From Torsvik et al., 2012 |
| Lower Lodeve sandstone | Norway | P | | 285 | | 3 | 7.7 | **−44.0** | **350.0** | | 168, T | From Torsvik et al., 2012 |
| Mount Hunneberg Sill | Sweden | P | | 285 | | 5 | 6.3 | **−38.0** | **346.0** | | 2211, T | From Torsvik et al., 2012 |
| Stabben Sill | Norway | P | | 291 | | 4 | 2.4 | **−32.0** | **354.0** | | 1540, T | From Torsvik et al., 2012 |
| Scania dolerites | Sweden | P | | 294 | | 5 | 6.5 | **−38.0** | **348.0** | | 2222, T | |

(*continued on next page*)

**Table 1** (*continued*)

| Rock Fm. | Location | Mag. | I corr. | Age Mag. | | Q | A95 | Pole | | EULER (270 Ma) | GPDB RefNo/Reference | Notes |
|---|---|---|---|---|---|---|---|---|---|---|---|---|
| | | | | Published | Est. | VdV | | Lat | Lon | (Baltica coord.) | | |
| | | | | | | | | | | | | From Torsvik et al., 2012 |
| Scania dolerite dikes | Sweden | P | | 294 | | 5 | 11 | **−37.0** | **354.0** | | 2211, T | From Torsvik et al., 2012 |
| Arendal diabase dykes | Norway | P | | 297 | | 3 | 7.1 | **−42.5** | **339.6** | | 175, T | From Torsvik et al., 2012 |
| Ny–Hellesund sills | Norway | P | | 297 | | 4 | 2.9 | **−39.0** | **341.0** | | 626, T | From Torsvik et al., 2012 |
| Donets basin | Ukraine | P | | 297 | | 6 | 3 | **−43.0** | **345.0** | | Iosifidi et al. (2010) | From Torsvik et al., 2012 |
| Svedlodarsk, Karamysh Fm. | Ukraine | P | | 299 | | 5 | 2.4 | **−48.4** | **349.8** | | Meijers et al. (2010) | From Torsvik et al., 2012 |
| Mount Billinger sill | Sweden | P | | 299 | | 5 | 4 | **−31.0** | **354.0** | | 2211, T | From Torsvik et al., 2012 |
| Kartamysh Fm., Donbas | Ukraine | P | | 299 | | 5 | 2.2 | **−48.2** | **348.3** | | Meijers et al. (2010) | From Torsvik et al., 2012 |
| Donets basin | Ukraine | P | | 301 | | 6 | 4 | **−42.0** | **359.0** | | Iosifidi et al. (2010) | From Torsvik et al., 2012 |
| Debaltsevo Donbas | Ukraine | P | | 303 | | 5 | 2 | **−48.2** | **342.3** | | Meijers et al. (2010) | From Torsvik et al., 2012 |
| Tashkovska Donbas | Ukraine | P | | 312 | | 5 | 2.9 | **−38.4** | **339.5** | | Meijers et al. (2010) | From Torsvik et al., 2012 |

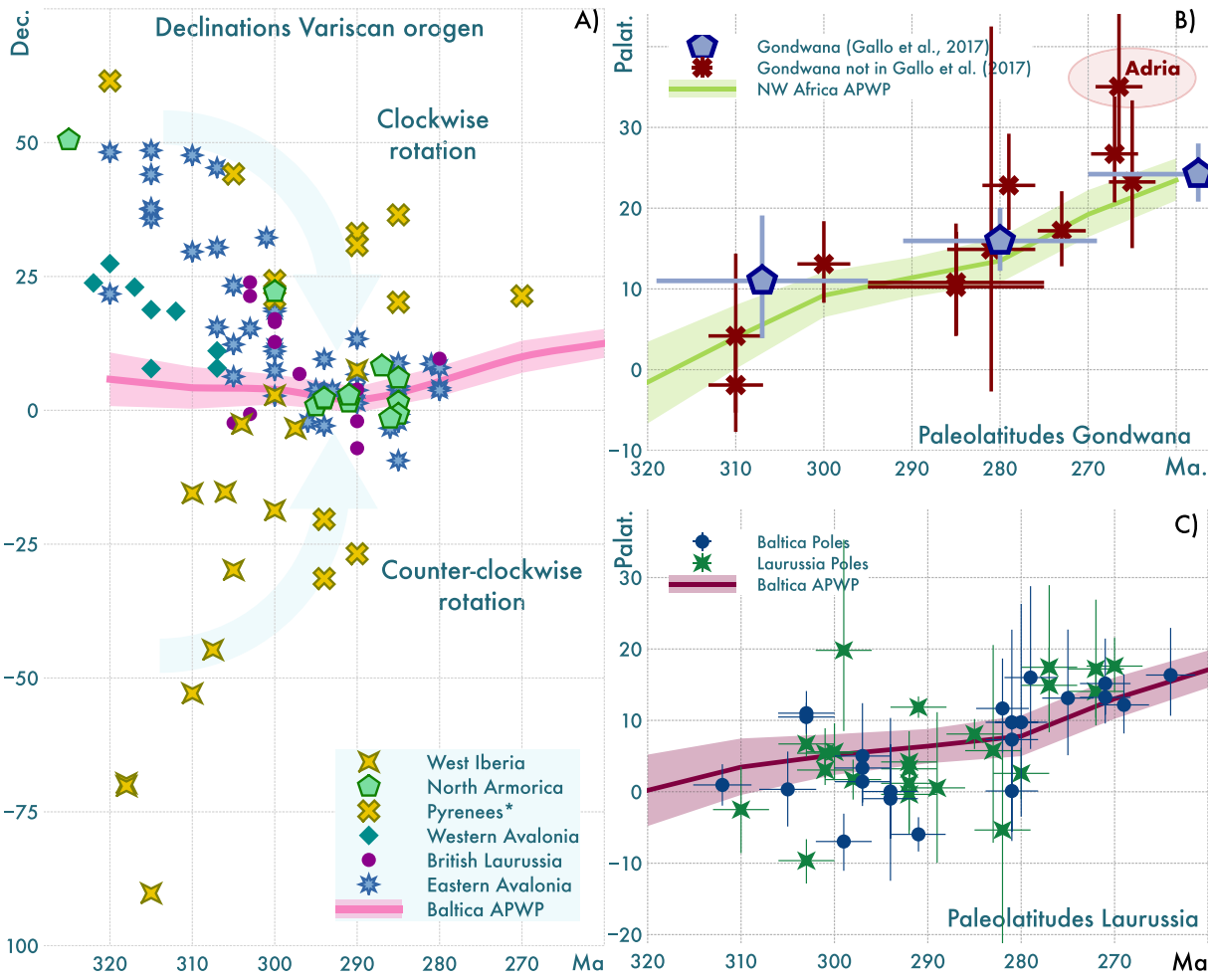


**Fig. 5.** (A) Plot showing the vertical axis rotations in the core of Pangea. expected declination of the studied paleomagnetic dataset from Europe and East North America compared with the global apparent polar wander path rotated to Baltica (Torsvik et al., 2012). A clockwise rotation of NW Europe and NE America and a counterclockwise rotation of the Iberian Peninsula and some areas of the Mediterranean are shown by the dataset. For errors see Fig. S1. B) Global Apparent Polar Wander Path (GAPWaP) rotated to the Gondwana coordinates and C) to and Laurussia A) shows poles from volcanic rocks and inclination corrected sedimentary rocks that were not included in Gallo et al. APWP. The only pole that does not fit is that from Adria (e.g., Kent and Muttoni, 2020) Reference location is county Cork, Ireland: 52° N, −9° E.

### *3.1. Pangea's first steps: Gondwana and Laurussia Paleozoic to Pennsylvanian*

During the Ediacaran, after Gondwana became its largest size (or the supercontinent Pannotia; see Murphy et al., 2021 and Evans, 2021 for a discussion), the Iapetus and Tornquist oceans opened (Robert et al., 2021) breaking apart the (super)continent. The opening of the latter ocean separated the Paleozoic Gondwana (to the south) from the northern continental masses, Laurentia and Baltica. During the Cambrian, a protracted period of rifting culminated with the opening of the Rheic Ocean in the Earliest Ordovician and the consequent separation of several micro-continents from the Gondwana margin (e.g., Nance et al., 2010), known as Avalonia *sensu lato* (including among others Avalonia *sensu stricto*, Ganderia, Carolinia, Meguma…). The mechanism (s) responsible for the Rheic Ocean opening is debated and includes slab-pull after Iapetus ridge subduction, slab roll-back underneath Gondwana or both (Murphy et al., 2006; van Staal et al., 2009; Díez Fernández et al., 2010; Pastor-Galán et al., 2013). The Iapetus and Tornquist oceans were consumed throughout the Ordovician and Silurian and Avalonia drifted northward towards Baltica and Laurentia until collision of the three landmasses during the Late Silurian–Early Devonian resulted in the Appalachian-Caledonide orogen (Van Staal et al., 1998; Mac Niocaill, 2000, Torsvik et al., 2012; Waldron et al., 2014; Fig. 2). At that time, the onset of closure of the Rheic Ocean had begun just after it reached its maximum width (~4000 km; Nance et al., 2010). The polarities of the Rheic subduction zones are disputed and include subduction towards Laurussia, Gondwana or both (e.g., Stampfli et al., 2013; Domeier and Torsvik, 2014 and references therein).

The Devonian-Carboniferous collision of Gondwana and the previously amalgamated Laurussia (Laurentia, Baltica and Avalonia), the two largest continents at the time, formed a large orogenic belt in the core of Pangea (Fig. 1). The collision zone became a 1000 km wide and 8000 km long global-scale orogenic system (Appalachian-Variscan-Alleghanian system) whose vestiges are now dispersed over Europe, Africa, and North America due to the Mesozoic break-up of Pangea (Fig. 2) (Domeier and Torsvik, 2014; Stampfli et al., 2013; Weil et al., 2013). The Variscan depicts a wavy trace (Fig. 2), being especially prominent the Greater Cantabrian (or Ibero-Armorican) Orocline (e.g., Weil et al., 2013) that draws a nearly 180° arc around and across the Bay of Biscay as it turns into northwest Iberia.

The Variscan formed because of the consumption of at least one major ocean, the Rheic, commencing at 420 Ma and whose mid-oceanic ridge subducted at ca. 395 Ma along its paleo-northern margin (Gutiérrez-Alonso et al., 2008a; Nance et al., 2010). The orogeny possibly involved some other large ocean(s) (Stampfli and Borel, 2002; Franke et al., 2017, 2020), but almost surely several minor oceanic

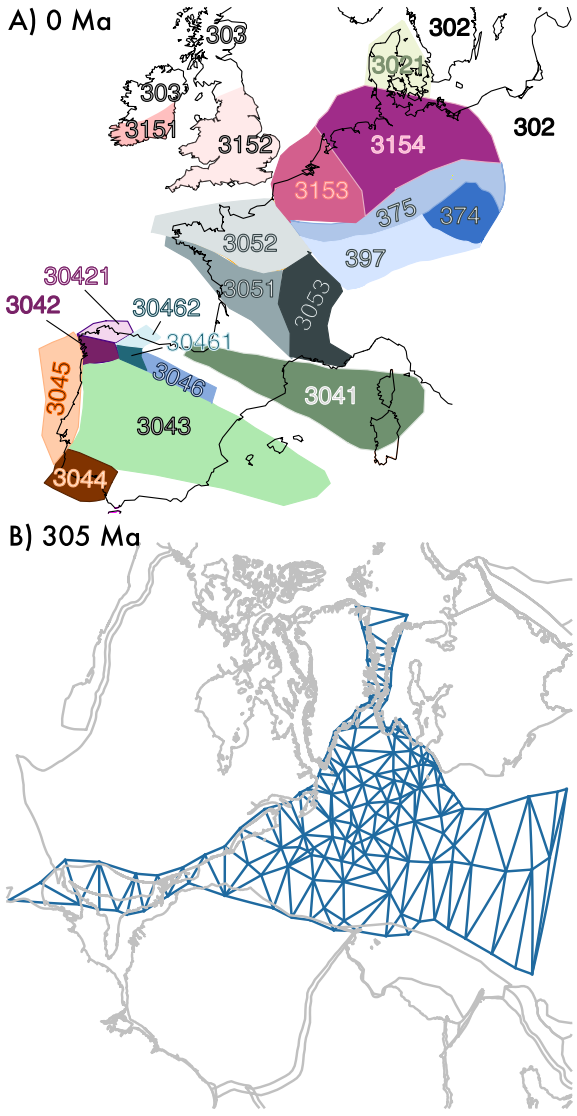


**Fig. 6.** A) Relation polygons modified from the continental network of CEED and their GPlates. B) The GPlates deforming topological network to visualize the intraplate deformation.

basins that existed between Gondwana, Laurussia, and other intervening microcontinents, closed during the Devonian-Carboniferous (e.g., Dallmeyer et al., 1997; Kroner and Romer, 2013; Pérez-Cáceres et al., 2017). The final continent-continent collision began once all oceans and intervening seaways were consumed. The commencement of the deformation was diachronous and became progressively younger westwards (in present-day coordinates) with Devonian continent-continent collisions along the eastern boundary, progressing to the earliest Permian ages in the westernmost sector (Hatcher, 2002; McWilliams et al., 2013; Chopin et al., 2014; Lopez-Carmona et al., 2014; Franke et al., 2017). Most tectonic reconstructions assume Pangea was a single and stable superplate from ca. 330 Ma (Domeier et al., 2012; Stampfli et al., 2013; Wu et al., 2021), when the architecture of the Variscan orogen begun to collapse in Europe (e.g., Vacek and Žák, 2019; Dias da Silva et al., 2021).

### 3.2. *The Pennsylvanian-Cisuralian events: Rheic westward closure and orocline buckling*

Despite the general assumption of a stable core of Pangea during Pennsylvanian times (<330 Ma), a western remnant of the Rheic ocean

**Table 2**
Relation of codes for different blocks used in the GPlates files.

| Plate ID # | Location | CEED parent Plate # | |
|---|---|---|---|
| 108 | East Avalonia | 101 | North America |
| 3021 | Denmark Peninsula | 302 | Baltic Shield |
| 303 | Northern Highlands | 302 | Baltic Shield |
| 304 | Iberia (Rigid) | 302 | Baltic Shield |
| 3041 | Pyrenees | 304 | Iberia |
| 3042 | Cantabrian Hinge | 304 | Iberia |
| 30,421 | Cantabrian Hinge | 304 | Iberia |
| 3043 | Central Iberia | 304 | Iberia |
| 3044 | South West Iberia | 304 | Iberia |
| 3045 | South West Iberia 2 | 304 | Iberia |
| 3046 | Cantabrian Zone (S) | 304 | Iberia |
| 30,461 | Cantabrian Zone North Hinge | 304 | Iberia |
| 30,462 | Cantabrian Zone NW Hinge | 304 | Iberia |
| 3051 | Central Europe | 305 | Armorica |
| 3052 | Central Europe | 305 | Armorica |
| 3053 | Central Europe | 305 | Armorica |
| 306 | France | 305 | Armorica |
| 3151 | Munster Basin | 315 | England Avalonia |
| 3152 | South Great Britain | 315 | England Avalonia |
| 3153 | NW Europe Avalonia | 315 | England Avalonia |
| 3154 | NE Europe Avalonia | 315 | England Avalonia |
| 3751 | German Variscan | 375 | Saxo Thuringia |
| 3752 | Central Europe Variscan | 375 | Saxo Thuringia |
| 1000 | Kazakhstan orocline | 302 | Baltic Shield |
| 1001 | Kazakhstan orocline | 302 | Baltic Shield |
| 1002 | Kazakhstan orocline | 302 | Baltic Shield |


**Fig. 7.** Location of major late Carboniferous and Early Permian extensional basins.

was still subducting and the Variscan orogen kept on evolving and deforming Pangea's core lithosphere (e.g., Hatcher et al., 2010; Murphy et al., 2016; Pastor-Galán et al., 2020; Wu et al., 2021). After the collapse of the European Variscan belt the Laurussia-dipping subduction likely ceased, whereas western Gondwana became or remained on the upper overriding plate until the final closure of the Rheic Ocean (e.g., Hatcher et al., 2010; Wu et al., 2021).

The final closure of the Rheic Ocean in North America commenced in the Pennsylvanian and ended in Cisuralian times (Alleghanian sector; Fig. 2; (e.g., Hatcher, 2002; Nance et al., 2010). In the northern Appalachians, Alleghanian orogenesis occurred as the result of oblique convergence between Laurentia and Gondwana and is dominated by dextral strike-slip on major northeast- and east-trending faults and vertical axis rotations (e.g., Nance et al., 2010; Warsame et al., 2021). The area underwent Barrovian metamorphism and records cooling ages of 320–295 Ma (Dallmeyer et al., 1986). In addition, there was coeval widespread anatectic granitoid magmatism (e.g., Hatcher et al., 2010). To the south, the Ouachita sector of the orogen (Fig. 2) shows no

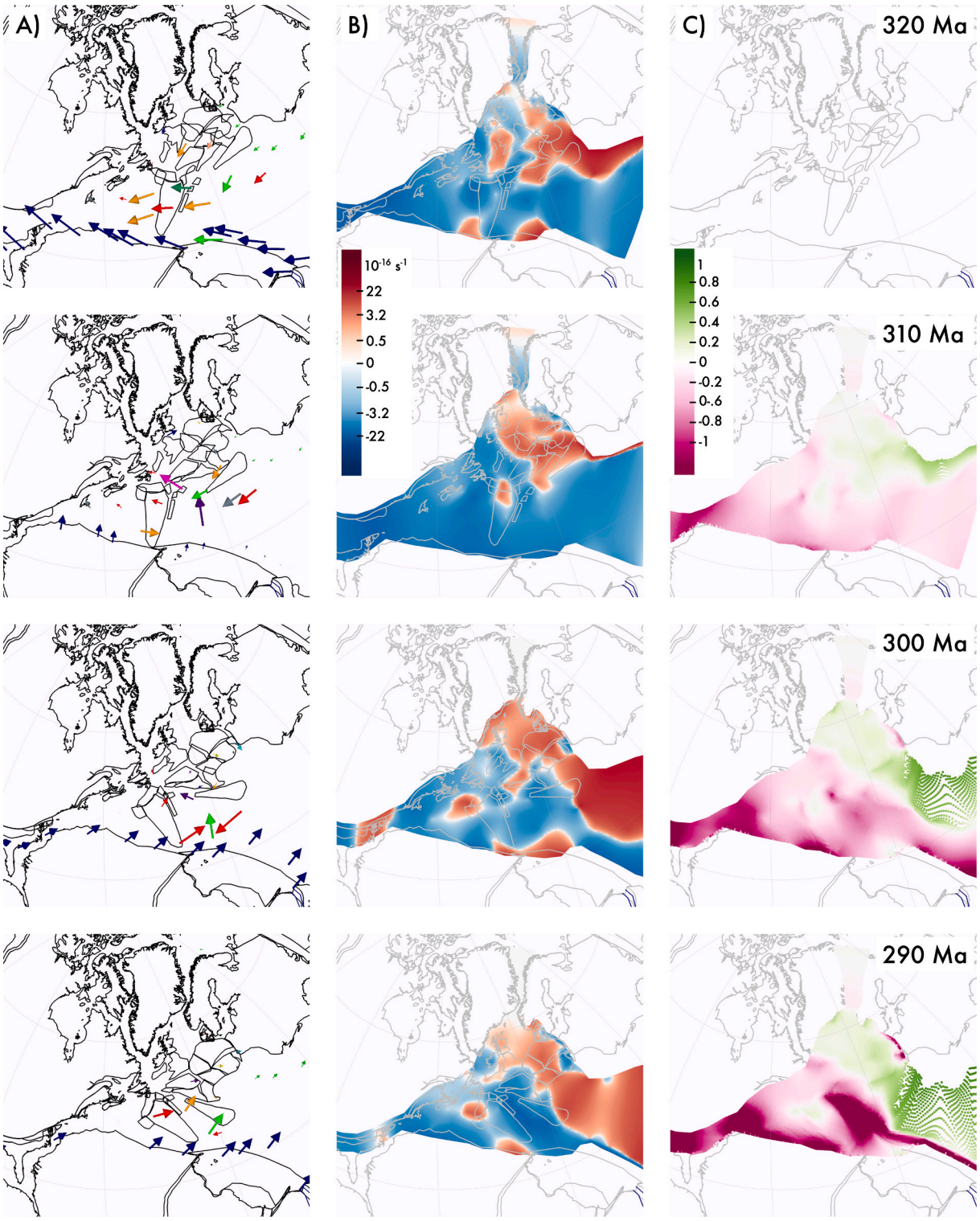


**Fig. 8.** Series of illustrations of the kinematic model at times 320 Ma, 310 Ma, 300 Ma and 290 Ma with Laurussia fixed. A) Polygon model showing the first step of the reconstruction where each polygon was treated as a rigid block. Arrows show the relative movements of selected centers of the polygons and Gondwana margins. B) Instantaneous strain rate at each time. Regions under extension are shown in light to dark red colors (depending on the strain rate, the darker the more extensional rate), whereas shortening is expressed in a scale of blue colors (the darker the higher shortening rate). C) Finite strain (accumulated amount of shortening or extension within the core of Pangea) at each of the considered times. The color code is shown as crustal thinning factor. This factor represents the changing crustal thickness (T) according to Crustal thinning factor = (1 - T/Ti) where 'Ti' is initial thickness. Values between 0 and 1 represent extended regions and negative values represent shortened regions. This factor starts with an initial value of 0 and has no units. (For interpretation of the references to colour in this figure legend, the reader is referred to the web version of this article.)

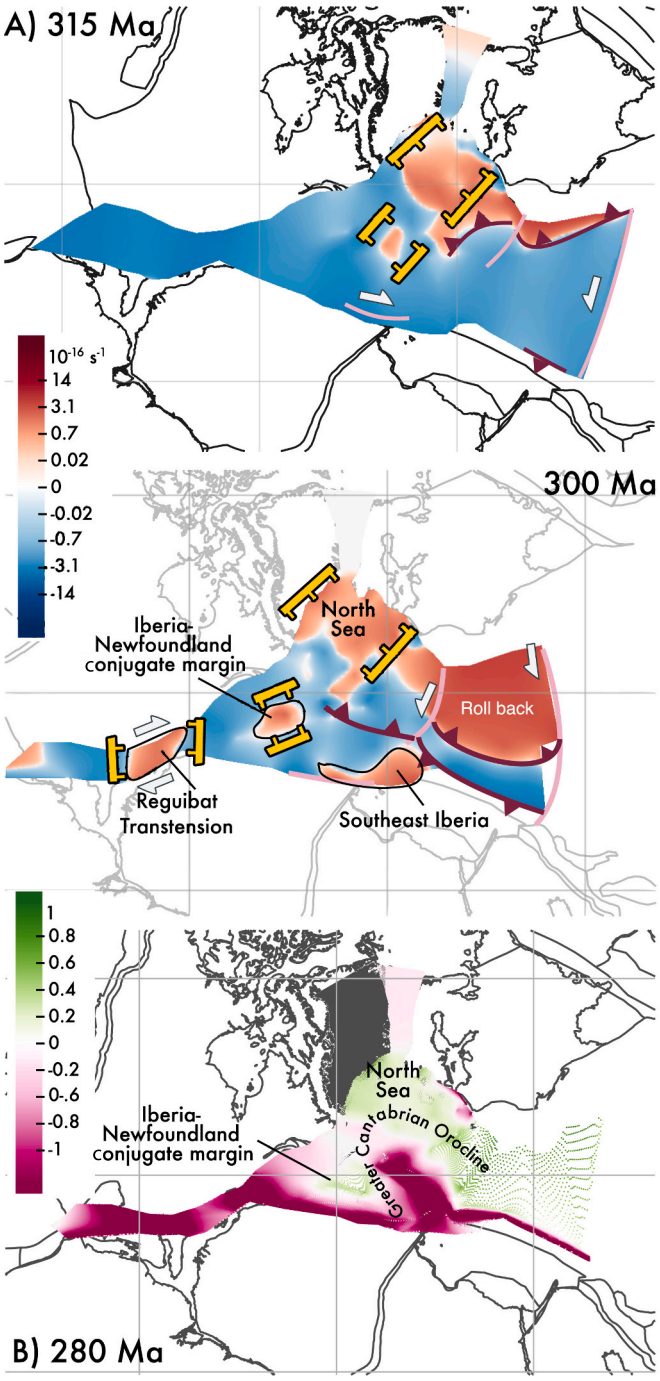


**Fig. 9.** Example of the interpretation of the plate deformation in the Core of Pangea. Continents are shown in white. Subduction zones are dark red lines with triangles, transforms and large shear zones are shown as light pink lines, and development of basins through extension with yellow bars. A) 315 Ma and 300 Ma instantaneous strain rate. B) Finite strain (at 280 Ma) within the deformable plate of inner Pangea. Color codes are as in Fig. 8. (For interpretation of the references to colour in this figure legend, the reader is referred to the web version of this article.)

metamorphic nor magmatic activity (see Nance et al., 2010 for details).

Hatcher (2002) and Hatcher et al. (2010) proposed that the Alleghanian collision between Gondwana and Laurentia began at the northeastern end of the Appalachians and closed the Rheic Ocean southward like a zipper. In this scenario, Gondwana rotated clockwise from the head-on collision with southeastern Laurentia in Pennsylvanian to Permian time, producing the Blue Ridge-Piedmont megathrust sheet and related foreland deformation from southern New York to Alabama (Hatcher, 2002).

Coeval with the final closure of the Rheic ocean in southwestern Laurussia (Alleghanian), the Variscan orogen of Europe underwent a final deformation phase which formed the Greater Cantabrian Orocline (e.g., Leite Mendes et al., 2021). The Greater Cantabrian Orocline (a.k.a. Ibero-Armorican Arc or Orocline) is arguably one the best studied oroclines on Earth (e.g., Weil et al., 2013; Gutiérrez-Alonso et al., 2015) and draws a "C" shape in western Europe from Brittany, Ireland across the Bay of Biscay into Iberia and it is particularly evident in northwestern Iberia (Fig. 2). All kinematic data studied so far support a model in which the Greater Cantabrian Orocline formed from a roughly linear belt after the collapse of the European Variscides through vertical-axis rotations in a period of time later than 315 Ma and earlier than 290 Ma. The southern limb of the orocline rotated counterclockwise (CCW) and the northern limb clockwise (CW, e.g., Weil et al., 2013). The main sources of data supporting the orocline formation are extensive paleomagnetic, structural and geochronological studies (e.g., Weil et al., 2013; Pastor-Galán et al., 2014; Shaw et al., 2015; Gutiérrez-Alonso et al., 2015).

### 3.3. *The two faces of Pangea*

A hypothesis of a Pangean superplate from ca. 330 Ma is not consistent with the kinematic, magmatic and metamorphic observations (e.g., Hatcher, 2002; Gutiérrez-Alonso et al., 2004; Johnston and Gutierrez-Alonso, 2010). In addition to the geological complications, paleolatitudes extracted from paleomagnetic data have consistently shown that there are problems with having a stable superplate since that time.

Pangea A refers to all models that resemble the classic Bullard fit (Bullard et al., 1965) of the continents before the opening of the Atlantic. All geological, geophysical and paleomagnetic data support a Pangea A during the Triassic and it is widely assumed that this was the shape for practically the entire lifespan (~330 to ~200 Ma) of the supercontinent (Fig. 1; e.g., Domeier et al., 2012; Torsvik et al., 2012). Since the 1960's (e.g., Van Hilten, 1964; De Boer, 1965) paleomagnetists have found that a Pangea A models produce large overlaps (>1000 km) during the Late Carboniferous and Permian times between Gondwana and Laurussia when using the paleolatitudes inferred from paleomagnetic data. To accommodate the paleolatitudes imposed by the paleomagnetic data, some authors suggested a different framework, a Pangea "B" model, in which Laurussia would have been located to the west of Gondwana (Fig. 1) (Gallo et al., 2017; Irving, 2004, 1977; Kent and Muttoni, 2020; Muttoni et al., 2003). The transition from a Late Carboniferous Pangea B to the unanimously agreed Pangea A configuration at the Permo-Triassic boundary (Kent and Muttoni, 2020; Müller et al., 2019) requires >3500 km of right-lateral displacement between Laurussia and Gondwana through one (or a series of) megashear zone(s) (Fig. 1).

Pangea B reconstructions acknowledge the internal mobility of Pangea during the Permian, but they are incompatible with the observed vertical axis rotations and associated shortening and extension in the interior of Pangea (Domeier et al., 2021, 2012). In addition, geologic evidence supporting Pangea B is lacking: Paleobiology evinces strong affinities between late Paleozoic flora of north-west Africa and western Europe–eastern North America (Correia and Murphy, 2020), similarities in Permian fauna in southern North America and northwestern South America, and affinities between the European Tethyan realm (Greater Adria) with central Asia (Angiolini et al., 2007). Stratigraphic and provenance analyses also link late Paleozoic sedimentary styles and facies between southern North America and northwestern South America, and between northern Africa and western Europe–eastern North America (Correia and Murphy, 2020; Domeier et al., 2012). Pangea B faces its most serious challenge in the absence of structural evidence for a ~ 3500 km dextral megashear zone between Gondwana and Laurussia. Despite the good exposure of the collision zone between

Gondwana and Laurussia, the only right lateral motion and shear zones are Carboniferous to Early Permian, rather than the necessary middle to late Permian age (Kent and Muttoni, 2020). In addition, right lateral motions estimated to be less than 1000 km (e.g., Matte, 2001; Waldron et al., 2015) are far below the necessary >3500 km. The Pangea B model also requires that southeastern North America (Ouachita) faced the Panthalassa Ocean (Fig. 1), the Appalachians were juxtaposed with the northern Andes, and the European Variscan opposed western Africa and closer to south America (Fig. 1). However, the paleontological and sedimentological evidence support a less mobile setting between the Laurussia-Gondwana pair within the Pangean supercontinent in the Late Carboniferous-Early Permian (e.g., Talavera-Mendoza et al., 2005; Correia and Murphy, 2020). Finally, most data support a tectonically stable Pangea interior from the Middle Permian (~270 Ma) to the Middle Triassic (~240 Ma) (Ziegler, 1990).

## 4. Kinematic constraints and model construction

The tectonic model is presented through this section together with a discussion of the underlying kinematic and paleogeographic constraints and its accordance with the geological data and interpretations.

### 4.1. Paleomagnetic constraints

Paleomagnetic data supports a general northward drift of Gondwana during the late Paleozoic. In contrast, Laurussia apparently maintained its latitude, perhaps moving roughly E-W, at least until the Early Permian (see Torsvik et al., 2012). From Early Permian, paleomagnetism from Laurussia suggests a northward movement together with Gondwana until the break-up of Pangea. Gallo et al. (2017) showed with a True Dipole analysis that the paleolatitudes for Baltica and Gondwana were compatible with Pangea A type between ~315 and 275 Ma. It is Laurentian and Gondwanan poles that do not fit. They support a B type model in which Baltica and Laurentia were decoupled during the late Carboniferous and early Permian. In this compilation, the poles from Laurentia that show a latitudinal misfit with Gondwana (Fig. 5; Table 1; Poles labeled in Table 1 as West Avalonia / Laurentia from Avalonia s.l. in the Atlantic Canada and northeast coast of the U. S.A.) are considered part of a deformable portion of inner Pangea since they show rotations compatible with those observed in the Variscan belt (Figs. 5 and 6, Table 2). Other middle to late Permian poles from North America fit adequately with Gondwanan poles apart from the observations from northern Italy (Adria poles) (e.g., Torsvik et al., 2012; Kent and Muttoni, 2020; Domeier et al., 2021).

Adria poles are, when considering the paleolatitudes, the most recurring ones in support of Pangea B. They are of good quality and abundant in contrast with the sparse poles from the rest of Gondwana (Domeier et al., 2021). Those poles have been used as a proxy for early Permian paleomagnetic data from Gondwana (Kent and Muttoni, 2020; Muttoni et al., 2009, 2003). However, Adria is thought to be a mobile microcontinent during the Mesozoic and Cenozoic (van Hinsbergen et al., 2020), and therefore may not properly represent Gondwana without an adequate correction (e.g., Domeier et al., 2021). In this paper I have averaged them all into one pole following Kent and Muttoni (2020), to avoid a bias towards their contested paleolatitude.

The reappraisal of the paleomagnetic observations from 330 Ma to 270 Ma in the Variscan orogen (Fig. 5; Table 1) shows vertical axis rotations with respect to the magnetic pole of continental blocks that affected the majority of the orogen, a vast area within Pangea (ca. $7.5 \times 10^6$ km$^2$; Figs. 1 & 2). This paleomagnetic dataset shows compatible paleolatitudes in the collision zone between Gondwana and Laurussia (Fig. 5; SF1). Data from NW Europe show a consistent ~30° clockwise rotation at 320 Ma. The magnitude of rotation decreases over time until it becomes 0 in all magnetizations younger than 270 Ma (Fig. 5) which are considered the upper and lower bounds for it. These rotations affected the majority of Gondwana and Avalonia s.l. (Fig. 1a former 'ribbon continent' that constituted the Laurussian southern realm (e.g., Nance et al., 2002; Cocks et al., 1997; Cocks and Fortey 2009). Late Carboniferous clockwise rotation also characterizes the original Laurentian margin (present day Scotland, and northern half of Ireland). However, the rotation is restricted to areas located in the vicinity of major structures active in the Carboniferous (Figs. 2 and 3) such as the Great Glen Fault (e.g., Speight and Mitchell, 1979; Elmore et al., 2006). Most of the Iberian Peninsula, SE France, Corsica and Sardinia show coeval and opposite sense (counterclockwise) rotations up to 90°. In the NW of the Iberian Peninsula, it is possible to observe, both in its geometry and through differential vertical axis rotations, the change in trend of the Variscan orogen of Europe (Fig. 1C; Weil et al., 2013) from SE-NW in Iberia to the WSW to ENE in the rest of Europe.

This review includes paleomagnetic datasets that were disregarded due to their secondary origin (i.e., data from older rocks that were remagnetized in the Carboniferous). In other cases, the observed rotations were considered either local effects, and therefore of minor significance in global tectonics (e.g., Edel et al., 2018) or supportive of Pangea B, despite showing no paleolatitude incompatibilities (Bachtadse et al., 2018). Despite its alleged stability, satisfying the late Carboniferous-early Permian vertical axis rotations implied by the paleomagnetic data require large-scale movements within Pangea. These movements would involve >1500 km of convergence and >1000 km extension accommodated somewhere within Pangea's interior (e.g., Pastor-Galán et al., 2018). The locations of this deformation have yet to be determined.

To satisfy the vertical axis rotations suggested by paleomagnetism, I have divided the Variscan belt into subterranes that all show similar net rotations with respect to Baltica (the stable continent with the largest and most consistent paleomagnetic dataset, Torsvik et al., 2012). The Euler poles were chosen to match the deformation imposed by the rotations in the reconstruction to the geological observations (see next section).

### 4.2. Geological data

The final consumption of the Rheic ocean relics and development of the Variscan orogen (s.l.) accommodated the oblique convergence between Gondwana and Laurussia during the Late Paleozoic (Nance et al., 2010; Murphy et al., 2016; Franke et al., 2017). At the end of the Carboniferous, the convergence imposed by the continuing northwards motion of Gondwana buckled the Variscan orogen forming the Greater Cantabrian Orocline (e.g., Leite Mendes et al., 2021). The orocline buckling process affected the margins of Gondwana and Laurussia, and likely accommodated several hundreds of kilometers of shortening on a lithospheric scale (Gutiérrez-Alonso et al., 2004; Gutiérrez-Alonso et al., 2012; Weil et al., 2013; Pastor-Galán et al., 2020. Late Carboniferous to early Permian shortening events are common in the European Variscides from east (Carpathians, e.g., Plissart et al., 2017) to west (Ireland, e.g., Quinn et al., 2005) coeval with ~50% of shortening of the North American segment of the orogen (Alleghanian), including a strong transpressive component (e.g., Hatcher et al., 2010). Similarly, coeval shortening characterizes the Mauritanides, the Variscan of NW Africa (Fig. 2; Chopin et al., 2014). Coeval convergence and shortening in the Central Asian Orogenic Belt (CAOB, Fig. 3; Safonova and Santosh, 2014) recorded the closure of the Turkestan Ocean (e.g., Xiao et al., 2015) and the bending/buckling of the Kazakhstan arc in the Central Asian Orogenic Belt (e.g., Li et al., 2018).

Widespread transpressional and transtensional lithospheric scale structures also formed between 320 and 270 Ma. The main strike-slip motion within the core of Pangea is right-lateral (Matte, 2001) owing to the E-W convergence imposed by Laurussia. Most of these faults follow the curved trend of the orogen suggesting accommodation of vertical axis rotations (Gutiérrez-Alonso et al., 2008a, 2015; Turrillot et al., 2011). Restoration of slip displacement along the faults brings the European Variscan belt into continuity with the Moroccan and North

American sections of the belt (Chopin et al., 2014; Gutiérrez-Alonso et al., 2008b; Weil et al., 2013). The Alleghanian orogen includes numerous dextral strike-slip faults such as the Minas fault that are inferred to have been continuous into Southern Europe and which were responsible for important local vertical axis rotations (Fig. 2; Warsame et al., 2021). These late Carboniferous early Permian strike-slip faults are common from Atlantic Canada to the central Appalachians (e.g., Hatcher et al., 2010).

In addition to shortening and wrenching, many areas of inner Pangea underwent extension that led to the formation of over 100 rift basins (Lamotte et al., 2015) (Fig. 7). Major Permian extensional and rift basins include the North Sea and Oslo rift, the Rotliegend areas (from the Netherlands to Poland, the large Karoo system extending from Arabia to South Africa, and the Neotethyan basin that opened along the south margin of the Paleo-Tethys ocean from Arabia to Australia (de Lamotte et al., 2015). Permian extension has been also documented at: (1) both Paleo-Tethyan north and south realms within the Variscan domain of Southern Iberia (e.g., Sánchez-Navas et al., 2017), the Alps and Adria (Pohl et al., 2018; Yuan et al., 2020; Molli et al., 2020) which has been interpreted as related to roll-back (Pereira et al., 2015, 2014) and (2) in localized areas along the Rheic suture including the Newfoundland-Iberia conjugate margin (Sandoval et al., 2019) and the Southern Appalachians (Ma et al., 2019) around the conjugate margin of the Reguibat promontory of Gondwana (Hatcher, 2002).

In Europe, a magmatic pulse that peaked at ca. 310–270 Ma has been recognized in the areas most affected by Late Carboniferous-Permian post-Variscan deformation. Voluminous mafic to granitoid intrusions were emplaced together with their extrusive equivalents across both the internal and external zones of the orogen (Boscaini et al., 2020; Gutiérrez-Alonso et al., 2011a; Wilson, 2004; Yuan et al., 2020). Similarly, a minor but relevant suite of gabbros with 310–300 Ma ages crop out in the Alleghanian from Virginia to South Carolina (Huebner and Hatcher, 2017). Although this magmatic event has been linked with the orogenic collapse of the Alleghenian–Variscan–Ouachita belt or with a plume, it is inconsistent with the age of the collapse of the Variscan belt in Europe, which finished by the earliest Pennsylvanian (Ballèvre et al., 2014; Dias da Silva et al., 2020; Franke, 2000; Martínez Catalán et al., 2009). Geochemical data from the Variscan magmatic rocks, especially in northern Europe, is not compatible with the involvement of a mantle plume (Gutiérrez-Alonso et al., 2008b).

In southern and western Europe, the magmatic pulse is compatible with subduction, delamination and/or slab break off (Boscaini et al., 2020; Gaggero et al., 2017; Pereira et al., 2014). Late Pennsylvanian to middle Permian rift basins show an extensive, but short-lived (305–270 Ma) magmatic pulse that accompanied extension (Ondrejka et al., 2018; Yuan et al., 2020; Zeh et al., 2000) that sometimes extended beyond the basin's margins (e.g., the Permian dyke and sill complexes of Northern England and Scotland; de Lamotte et al., 2015). In the case of the Neotethys rifting, plume volcanism was possibly involved. The Panjal Traps of present-day NW India, was emplaced at 289 ± 3Ma in the southern realm of the Paleotethys ocean (Yeh and Shellnutt, 2016), and possibly aided lithospheric extension and opening and of the Neotethys ocean.

High Pressure (HP) metamorphism, ophiolite obduction and arc inception occurred along the Paleotethys realm from at least the Caucasus to China, between 320 and 270 Ma (Jian et al., 2008; Rolland, 2017; Rolland et al., 2016; Shafaii Moghadam and Stern, 2014; Zhang et al., 2016). Subduction initiation and/or ridge subduction events accommodated the northwards movement of Gondwana and the plate reorganization after the formation of the Pangean supercontinent. Subduction initiation/ridge subduction of the Paleotethys was coeval with the rifting of the Neotethys (e.g., Gutiérrez-Alonso et al., 2008b). The latter subduction and obduction record together with the Late Carboniferous and Permian development of the Meliata Arc, in eastern Europe, suggest a northward directed subduction initiation and/or ridge subduction. In contrast, arc magmatism in the Pontides (present day Turkey) records south-dipping Paleotethyan subduction beneath Greater Adria (Fig. 10; van Hinsbergen et al., 2020). Other relics of southward subduction have not been found along the Paleotethyan southern realm.

Coeval HP metamorphism occurred in the Central Asian Orogenic Belt (CAOB; Fig. 3) and along the margins of Panthalassa (Nipponides)

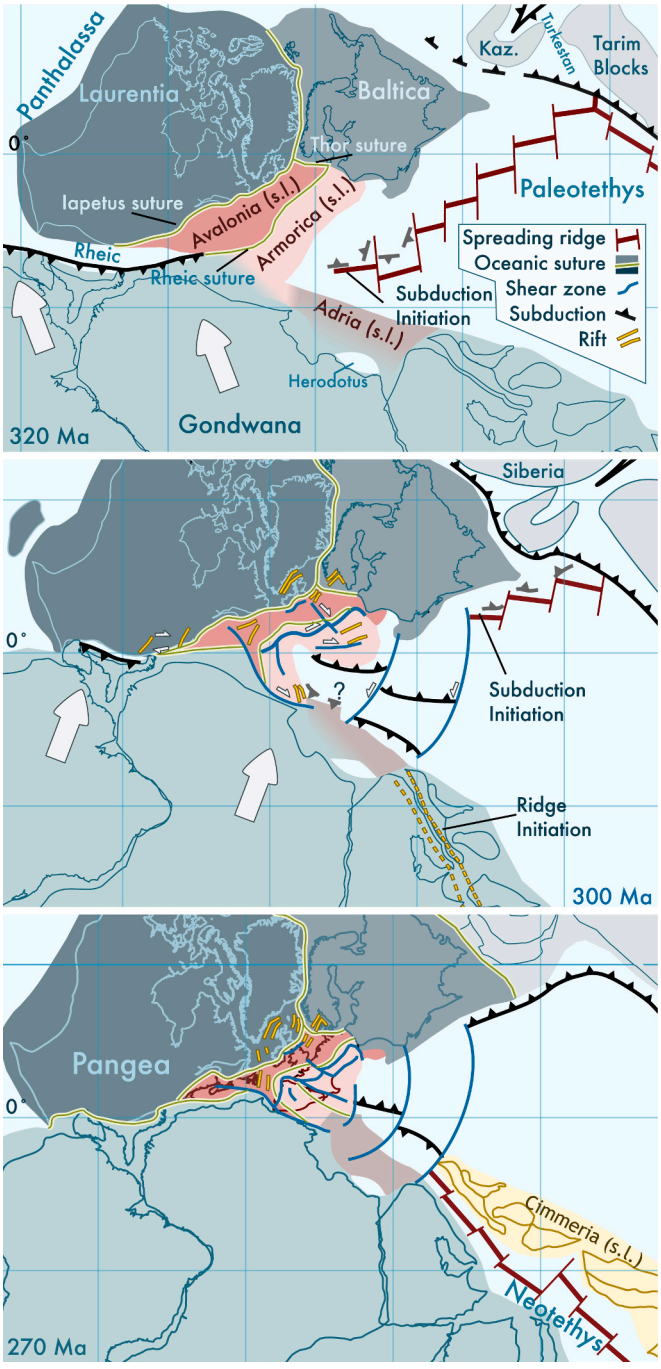


**Fig. 10.** Formation of Pangea. Plate reconstruction of the core of Pangea. The continuing northwards convergence of Gondwana leading to a change in the stress field in the Variscan orogen, which produced shortening, vertical axis rotations and localized extension. Synchronous subduction initiation/ridge failure/ridge subduction occurred in the Paleotethys around 300 Ma. After the opening of the Neotethys, migration of Cimmeria northwards, and amalgamation of Siberia craton to Laurussia, Pangea became a rigid superplate by about 270 Ma. The lithospheric scale structures formed during the period 320–270 Ma may explain why Pangea broke up where it did in the North Atlantic did not follow the previous sutures.

(Isozaki et al., 2010; Li et al., 2018). A particular feature of the late Carboniferous and Permian HP metamorphic rocks is a global lull in the occurrence of lawsonite blueschists (Tsujimori and Ernst, 2014). This lawsonite hiatus may be an indication of a warm thermal regime in the subduction zones at that time (Tsujimori and Ernst, 2014).

### 4.3. Model construction

The building process of the kinematic model is summarized by Figs. 8 and 9. Fig. 8 shows three columns of snapshots at 320, 310, 300 and 290 Ma. Column A shows the initial stage with the selected polygons that acted as 'rigid blocks' to accommodate the rotations inferred from paleomagnetic data. Column B represents the instantaneous strain rate within the deformable plate (Fig. 6), in other words how much compression or extension the model is predicting at the selected times. Column C depicts the accumulated strain at each time. Fig. 9 shows how the plate boundaries and major faults were located following the results of Fig. 8.

In the model presented herein, the Euler poles describing the rotations inferred from the paleomagnetic data have been iteratively modified in such way that the strain rates and finite strain predicted by the model match the geological observations (Figs. 8, 9, and 10; Suplementary Datafile S2). For example, when the kinematic model predicts extension (Fig. 8 B and C in the North Sea or between Iberia and Atlantic Canada), I have fitted the Euler poles to match with the orientation and magnitude of areas of extension. The extension has been distributed to match the finite extension (~20%, Figs. 8 and 9), subsidence and/or rifting volcanism observed in those basins during the latest Carboniferous and Early Permian (e.g., Sandoval et al., 2019; Fossen et al., 2021). Likewise, where shortening or convergence is predicted by the model (Figs. 8C and 9), I have matched it with the best available candidates. In the case of the westernmost tip of the Paleotethys ocean (Figs. 9 and 10) I had to accommodate a large amount of convergence. In the widest affected area (southeastern Europe and the Greater Adria realm in Figs. 8 and 10) the simplest solution was two subduction zones, one with polarity towards Gondwana (Figs. 9 and 10), which fits with the arc volcanism found in the Pontides in Turkey (van Hinsbergen et al., 2020) and one with polarity to the north that rolled-back forming a large back-arc basin. Although the Greater Cantabrian Orocline show certain amount of shortening during its formation (e.g., Pastor-Galán et al., 2020), such shortening is not enough to explain all the convergence of the kinematic model (Figs. 8 and 9). To accommodate such missing convergence, I have added a subduction zone with polarity to the north (under the present-day Pyrenees) that rolled-back explaining observed vertical axis rotations and magmatism. In the reconstruction, the Paleotethyan subduction has been reconstructed as segmented with different polarities (Figs. 9 and 10) as it was the simplest kinematic solution fitting the present-day datasets. However, subduction with other polarities may have occurred along parts of the northern and southern margins of the Paleotethys.

## 5. Discussion

Most geologic syntheses propose that Pangea amalgamated at ~330 Ma and remained stable for over 130 Myr as a single quasi-rigid plate until its early Jurassic break-up. Despite consensus on the Pangea A configuration (e.g., Domeier et al., 2012, 2021), the structural, petrologic and geochronologic data reviewed here, suggest that substantial areas of Pangea were intensively internally deformed during the late Carboniferous and early to middle Permian (e.g., Casale et al., 2017; Jacques et al., 2018; Leary et al., 2017; Quinn et al., 2005; Rolland et al., 2016) and become internally stable at ca. 270 Ma (e.g., Gutiérrez-Alonso et al., 2008b; van Hinsbergen et al., 2020). During that time interval: (1) large amounts of lithospheric-scale shortening formed or modified orogenic belts in western Europe, North Africa and southeastern North America (Chopin et al., 2014; Pastor-Galán et al., 2020, 2018); (2) voluminous post-collision magmatism occurred in the Variscan belt (Boscaini et al., 2020; Gaggero et al., 2017); (3) oceanic rocks within the intra-Pangea Paleotethys ocean were obducted and exhumed (Zi et al., 2012); (4) extension and rifting occurred in the present day North Sea, Atlantic Canada-Iberia conjugate margins, eastern Africa and west Australia, and the southern realm of the Paleotethys, which, after a protracted extension, gave rise to the formation of a ribbon continent (Cimmeria) and the opening of the Neotethys Ocean (de Lamotte et al., 2015).

### 5.1. Kinematic model

The kinematic model starts following previous models in which Gondwana, following a northwards trajectory through the late Paleozoic (~400 to 250 Ma) (e.g., Torsvik and Cocks, 2017; Stampfli et al., 2013; Domeier and Torsvik, 2014; Wu et al., 2021), and Laurussia, moving E-W during Carboniferous times (~360 to ~300 Ma) (e.g., Torsvik et al., 2012), collided forming a diachronous westward-younging orogen (e.g., Edel et al., 2018; Wu et al., 2021) from Late Devonian (in eastern Europe) to the early Permian (southeastern North America) (e.g., Nance et al., 2010).

I propose a kinematic model in which the Pangea supercontinent kept on deforming for at least 50 myr (Fig. 8). During the late Carboniferous, the deformation along the increasingly coupled Gondwana and Laurussia boundary could no longer accommodate the rapid northwards motion of Gondwana on the orogen's eastern side, whereas the subduction of the Rheic ocean accommodated the convergence of its western realm. The western Rheic remnant subduction allowed the slight clockwise rotation of Gondwana, as suggested by paleomagnetic data (Gallo et al., 2017; Torsvik et al., 2012). The rotation of Gondwana produced a buttress effect (see Hatcher, 2002), which together with the protracted northwards convergence, led to a change in the stress field, buckling the previously formed orogen in the Rheic western realm between 320 Ma and 270 Ma (e.g., Gutiérrez-Alonso et al., 2004; Pastor-Galán et al., 2012).

This reconstruction of the core of Pangea between 320 and 270 Ma reconciles the paleomagnetic observations (Fig. 5) predicting >1500 km of shortening and extension in the core of Pangea and the mechanisms responsible for such deformation occurred (Pastor-Galán et al., 2018) (Figs. 8 and 9). The model recognizes the formation of an orogen-scale orocline (Greater Cantabrian Orocline, Weil et al., 2013; Leite Mendes et al., 2021) that accommodates part of the shortening by plate deformation within Pangea and part by subduction initiation and roll-back in the Paleotethys (Figs. 9 and 10). The continental shortening led to major vertical axis rotations (Fig. 5A) in Iberia, NW Africa, British Isles, and the Alleghanian orogen (Chopin et al., 2014; Hatcher, 2002; Merino-Tomé et al., 2009; Quinn et al., 2005; Warsame et al., 2021). In contrast, most of the extension is concentrated in the North Sea, The Iberia-Newfoundland conjugate margin and in the southeastern Alleghanian orogen (de Lamotte et al., 2015; Ma et al., 2019; Sandoval et al., 2019). The widespread magmatic activity in the core of Pangea within the time frame 320 to 270 Ma is consistent with a hemispheric subduction initiation within the Paleotethys ocean (Gutiérrez-Alonso et al., 2008b; van Hinsbergen et al., 2020). Subduction initiation and/or ridge subduction along the northern margin of the Paleotethys ocean (e.g., Gutiérrez-Alonso et al., 2008b; Jian et al., 2008; Rolland, 2017; Rolland et al., 2016; Shafaii Moghadam and Stern, 2014; Zhang et al., 2016), accommodated convergence within the Paleotethys and triggered major slab pull and roll-back in the north and southern Paleotethyan realms (Fig. 10 and Supplementary Videos). Both processes (slab-pull and roll-back), perhaps together, could be responsible for initiating the opening of the Neotethys Ocean during the early to mid-Permian (290–270 Ma) after Cimmeria rifted apart from Gondwana (Domeier and Torsvik, 2014; Gutiérrez-Alonso et al., 2008b). From 270 Ma, the northward migration of Cimmeria and the enhanced subduction of the Paleotethys accommodated most of Gondwana convergence, establishing the new

plate kinematic system. At that time, all available geological and paleomagnetic data suggest that Pangea became a rigid superplate until about 240 Ma, when extension began culminating in the nucleation of the future central Atlantic Ocean, which opened ca. 200 Ma (Müller et al., 2019). The sustained northwards convergence of Gondwana with Laurussia and the northern realm of the Paleotethys likely contributed to the buckling of the Kazakhstan arc and closing of the western Central Asian Orogenic belt in the Permian (Li et al., 2018) (Fig. 10 and Supplementary Videos).

Subduction initiation/ridge subduction along the Paleotethys can explain the hiatus of lawsonite blueschists during the Permian (Tsujimori and Ernst, 2014). The absence of lawsonite in high pressure rocks indicates hotter subduction zones, for example during subduction of the youngest ocean lithosphere. In addition, the model presented herein allows speculation about the effect of these newly developed subduction zones on processes near the core-mantle boundary. The subduction zones developed in the Paleotethyan realm occurred over the large indent in the northern area of the LLSVP TUZO (Burke, 2011; Burke et al., 2008) evoking the possibility of a cause-effect relationship (Fig. 4). Permian subducting slabs of the Paleotethys might have modified the shape of this low shear velocity province after descending into it.

Finally, the kinematic model gives a first insight to explain why Pangea did not separate in Europe along the sutures of the former Iapetus/Rheic oceans as predicted by a traditional view of the Wilson cycle (Fig. 1). The subduction in the western apex of the Paleotethys, the early extension in the Newfoundland-Iberia conjugated margin, and the large, curved strike-slip faults formed around the Greater Cantabrian orocline may have created the lithospheric weaknesses necessary to facilitate the break-up of Pangea and the opening of the Atlantic and Bay of Biscay.

### 5.2. Pangea's A, B, C…

There is vast geologic and geophysical support for the Wegenerian Pangea A (Fig. 1) configuration from the Triassic. Paleomagnetic data has been difficult to reconcile with this A type reconstruction for pre-Late Triassic time (Domeier et al., 2012). The proposal of a Pangea B (Fig. 1; Irving, 1977) solved the paleolatitudinal problems, but was inconsistent with the geological record. Some paleomagnetists suggested unconventional solutions to match the data (non-dipolar fields, bias in the record, assumptions of inclination shallowing; see Domeier et al., 2012 and Kent and Muttoni, 2020, for a review and discussion). The True Dipole analysis by Gallo et al. (2017) got rid of all the unconventional solutions and show that paleolatitudes for Baltica (with the best known paleomagnetic record at the time, Torsvik et al., 2012) and Gondwana were compatible with Pangea A type, but not those of Laurentia and Gondwana. The analysis of Gallo et al., include only 4 paleomagnetic poles from Laurentia in the interval between ~315 and 275 Ma. All those poles show vertical axis rotations (Fig. 5; Table 1) consistent with paleomagnetic data in Nova Scotia (Warsame et al., 2021) and coherent with the rest of the Variscan belt. Therefore, I have included those areas within the deformable core of Pangea.

The recognition of major late Carboniferous - early Permian continental-scale deformation and subduction initiation in the Paleotethys is consistent with paleomagnetic datasets (Fig. 5 and Table 1) and with the late Carboniferous and Permian geologic database. The kinematic reconstruction presented here has two versions to account for the potential paleolatitudinal overlaps inferred from paleomagnetic data (see Gallo et al., 2017). None of the alternatives require a Pangea B setting at any time between 320 Ma and 270 Ma. Both models show a good fit between the GAPWaP (Torsvik et al., 2012), the individual poles and Gallo et al. (2017) APWP for Gondwana (Fig. 5), except for poles from Adria, which have been ruled out since they seem to not be a good proxy for Gondwana's paleolatitude (van Hinsbergen et al., 2020; Domeier et al., 2021). This reconstruction shows no overlapping of continents due to incompatible paleolatitudes (Figs. 5 and 10), and therefore removes the need to invoke >3500 km of an intra-Pangean dextral megashear (Bachtadse et al., 2018; Kent and Muttoni, 2020) during the Permian, which has never been documented.

### 5.3. Pangea and the supercontinent cycle

The supercontinent cycle was originally suggested based on the age distribution of orogens, where the peaks in formation of orogens were attributed to amalgamation of supercontinents. This idea has been further grounded on indirect geochemical and geochronological proxies whose signatures are not always equivalent (Spencer et al., 2013), mostly because of the limitations of plate reconstructions in pre-Jurassic times (Evans, 2013; Domeier and Torsvik, 2019). The difficulties in identifying which and when landmasses became supercontinents is, in part, a matter of definition (see Pastor-Galán et al., 2019 for a discussion on definitions). The amalgamation and disruption of supercontinents have been linked to paleogeographical changes in sea-level, biogeochemistry and global climate change (e.g., Nance et al., 1988; Campbell and Allen, 2008). Such external changes do not require any predetermined geodynamic setting, the mere existence of one supercontinent (in the sense of an unusually large landmass) and its counter super-ocean would trigger most of them. In contrast, geochemical proxies (Gardiner et al., 2016; Spencer et al., 2013); numerical models (Gurnis, 1988; Coltice et al., 2009; Heron and Lowman, 2010; Yoshida and Santosh, 2011; Heron, 2019) and variations of the geomagnetic field (Eide and Torsvik, 1996) suggest that the formation of supercontinents may control the mantle geodynamics and the global plate tectonic circuits. These potential links led to the development of a supercontinent cycle hypothesis that would drive the long-term solid Earth's geodynamics tied to large igneous provinces (LIPs), plume volcanism, deep mantle circulation, outer core dynamics and the evolution of Earth's magnetic field (Nance et al., 2014; Heron, 2019; Pastor-Galán et al., 2019: Mitchell et al., 2021). However, and despite their potential importance, all these links remain permissive rather than proven.

Most proposals tying supercontinents to mantle circulation assume that the supercontinents cover 15–20% of Earth's surface and are superplates with no internal lithosphere-mantle interactions for long periods of time (usually >75 Myr) (Coltice et al., 2007, 2009; Heron, 2019; Pastor-Galán et al., 2019). When a plate achieves a large enough size, it may act as a lid limiting effective cooling of the underlying mantle. The development of hot mantle beneath such a lid could explain the CAMP plume (e.g., Coltice et al., 2007; Denyszyn et al., 2018). Superplates that limit interactions with the underlying mantle would also lead to reorganization of the plate tectonic circuits including a rapid redistribution of subduction zones and spreading ridges. It may also change the distribution of mass in the Earth's mantle and induce TPW events. In turn, the sometimes-invoked peripheral subduction ring as a driver of the supercontinental cycle, does not require a continental superplate and can occur at any stage of the supercontinent cycle (for example the Pacific ring of fire).

My kinematic reconstruction acknowledges that Pangea acted as supercontinent (in the sense of continuous land mass) for over about 130 Myr (330 to 200 Ma), which may have had a significant influence on external geological processes such as changes in sea-level, biogeochemistry, and global climate. In contrast to being a single and rigid plate, the supercontinent was still divided into fragments that interacted with each other and with the underlying asthenosphere until ~270 Ma. The 240 Ma initiation of extension within Pangea culminated in central Atlantic rifting at 200 Ma (Müller et al., 2019). Therefore, in this model, plates amalgamated into a Pangea superplate for less than 70 Myr. Following this scenario, Pangea acted as a superplate for a relatively short period of time, compared to the time it was a supercontinent. The suggested superplate lifespan may be too short to be a major influence on the mantle and core geodynamics that conceptual and numerical models predict for supercontinents acting as an insulating lid (Coltice

et al., 2009; Heron, 2019; Yoshida and Santosh, 2011).

The tectonic reconstruction presented in this paper begs for a reassessment of Pangea as a template for other supercontinents or for the supercontinent cycle itself. It is fair to state that whereas numerical modelling provides relevant insights on supercontinent signatures on mantle and lithosphere (e.g., Rolf et al., 2012, Yoshida and Santosh, 2011), model outcomes are too sensitive to changes in rheological parameters (e.g., Heron et al., 2021). It seems intuitive that larger continental plates would have larger imprints on the evolution of the inner Earth. A possibility is that there is no superplate size and lifespan threshold necessary to trigger a supercontinental cycle, but a progressively larger influence with size and time, opening the doors to disputed supercontinents (as Pannotia) as having had important roles in the cycle.

## 6. Conclusions

- The first phase of the collision between Gondwana and Laurussia formed the supercontinent Pangea ~330 Ma. However, the interior of Pangea remained tectonically active and deforming until it became a superplate 270 Ma.
- The establishment of the Pangea superplate caused a plate reorganization.
- The kinematic scenario in this paper reconciles the controversial Late Carboniferous - Permian paleomagnetic database and the geological record without summoning unobserved megashear zones (as in Pangea B), nor unjustified paleomagnetic issues to support a Pangea A superplate from 330 Ma (non-dipolar contributions; assumptions on inclination shallowing…)
- Pangea was a superplate for a relatively short time (<70 Myr), perhaps too short to have a strong influence on the mantle circulation.

Supplementary data to this article can be found online at https://doi.org/10.1016/j.earscirev.2022.103918.

## Declaration of Competing Interest

The authors declare that they have no known competing financial interests or personal relationships that could have appeared to influence the work reported in this paper.

## Acknowledgments

Thorough and constructive reviews by J. Brendan Murphy and an anonymous reviewer improved greatly this paper. I would like to acknowledge (in alphabetical order) Mark Dekkers, John Geissman, Gabriel Gutiérrez-Alonso, Stephen Johnston, Cor Langereis, Patrick Meere, Tatsuki Tsujimori, and Rob van der Voo for endless discussions about the reconstruction. This paper is a contribution to UNESCO's IGCP 648: Supercontinent Cycles & Global Geodynamics project and it is dedicated to the career of Rob van der Voo. This work has been funded by a post-doctoral fellowship from The Netherlands Research Centre for Integrated Solid Earth Sciences (ISES), a fellowship for overseas researchers from the Japan Society for Promotion of Science (JSPS) (grant P16329) and a MEXT/JSPS KAKENHI Grant (JP16F16329) and a Ramón y Cajal Fellowship from the Spanish Ministry of Science and Innovation. I especially thank all the beats Charles Robert Watts has ever made. The author declares no competing interest.

## References

Angiolini, L., Gaetani, M., Muttoni, G., Stephenson, M.H., Zanchi, A., 2007. Tethyan oceanic currents and climate gradients 300 m.y. ago. Geology 35, 1071–1074. https://doi.org/10.1130/G24031A.1.

Bachtadse, V., Aubele, K., Muttoni, G., Ronchi, A., Kirscher, U., Kent, D.V., 2018. New early Permian paleopoles from Sardinia confirm intra-Pangea mobility. Tectonophysics 749, 21–34. https://doi.org/10.1016/J.TECTO.2018.10.012.

Ballèvre, M., Martinez Catalan, J.R., Lopez-Carmona, A., Pitra, P., Abati, J., Fernandez, R.D., Ducassou, C., Arenas, R., Bosse, V., Castineiras, P., Fernandez-Suarez, J., Gomez Barreiro, J., Paquette, J.-L., Peucat, J.-J., Poujol, M., Ruffet, G., Sanchez Martinez, S., 2014. Correlation of the nappe stack in the Ibero-Armorican arc across the Bay of Biscay: a joint French-Spanish project. Geol. Soc. Lond., Spec. Publ. 77–113 https://doi.org/10.1144/SP405.13.

Belica, M.E., Tohver, E., Pisarevsky, S.A., Jourdan, F., Denyszyn, S., George, A.D., 2017. Middle Permian paleomagnetism of the Sydney Basin Eastern Gondwana: Testing Pangea models and the timing of the end of the Kiaman Reverse Superchron. Tectonophysics 699, 178–198.

Bilardello, D., Kodama, K.P., 2010. A new inclination shallowing correction of the Mauch Chunk Formation of Pennsylvania, based on high-field AIR results: Implications for the Carboniferous North American APW path and Pangea reconstructions. Earth Planet. Sci. Lett. 299, 218–227. https://doi.org/10.1016/j.epsl.2010.09.002.

Bilardello, D., Kodama, K.P., 2010. Rock magnetic evidence for inclination shallowing in the early Carboniferous Deer Lake Group red beds of western Newfoundland. Geophy. J. Inter. 181 (1), 275–289.

Boscaini, A., Marzoli, A., Davies, J.F.H.L., Chiaradia, M., Bertrand, H., Zanetti, A., Visonà, D., De Min, A., Jourdan, F., 2020. Permian post-collisional basic magmatism from Corsica to the Southeastern Alps. Lithos 376–377, 105733. https://doi.org/10.1016/j.lithos.2020.105733.

Boyden, J.A., Müller, R.D., Gurnis, M., Torsvik, T.H., Clark, J.A., Turner, M., Ivey-Law, H., Watson, R.J., Cannon, J.S., 2011. Next-generation plate-tectonic reconstructions using GPlates. In: Keller, G.R., Baru, C. (Eds.), Geoinformatics: Cyberinfrastructure for the Solid Earth Sciences. Cambridge University Press, Cambridge, pp. 95–113.

Bullard, E., Everett, J.E., Gilbert Smith, A., 1965. The fit of the continents around the Atlantic. Philos. Trans. Royal Soc. London. Series A, Math. Phys. Sci. 258 (1088), 41–51.

Burke, K., 2011. Plate tectonics, the Wilson Cycle, and Mantle Plumes: geodynamics from the top, annual review of earth and planetary sciences. Ann. Rev. https://doi.org/10.1146/annurev-earth-040809-152521.

Burke, K., Steinberger, B., Torsvik, T.H., Smethurst, M.A., 2008. Plume Generation Zones at the margins of Large Low Shear Velocity Provinces on the core-mantle boundary. Earth Planet. Sci. Lett. 265, 49–60. https://doi.org/10.1016/j.epsl.2007.09.042.

Campbell, I.H., Allen, C.M., 2008. Formation of supercontinents linked to increases in atmospheric oxygen. Nat. Geosci. 1, 554–558. https://doi.org/10.1038/ngeo259.

Casale, G., Levine, J.S.F., Craig, T.D., Stewart, C., 2017. Timing and deformation conditions of the Tallulah Falls dome, NE Georgia: Implications for the Alleghanian orogeny. GSA Bull. 129, 1195–1208. https://doi.org/10.1130/B31595.1.

Chopin, F., Corsini, M., Schulmann, K., El Houicha, M., Ghienne, J.-F., Edel, J.-B., 2014. Tectonic evolution of the Rehamna metamorphic dome (Morocco) in the context of the Alleghanian-Variscan orogeny. Tectonics 33, 1154–1177. https://doi.org/10.1002/2014TC003539.

Cocks, L.R.M., McKerrow, W.S., Van Staal, C.R., 1997. The margins of Avalonia. Geol. Mag. 134 (5), 627–636.

Cocks, L.R.M., Fortey, R.A., 2009. Avalonia: a long-lived terrane in the Lower Palaeozoic?. Geological Society, London. Special Publications 325 (1), 141–155.

Coltice, N., Phillips, B.R., Bertrand, H., Ricard, Y., Rey, P., 2007. Global warming of the mantle at the origin of flood basalts over supercontinents. Geology 35, 391–394. https://doi.org/10.1130/G23240A.1.

Coltice, N., Bertrand, H., Rey, P., Jourdan, F., Phillips, B.R., Ricard, Y., 2009. Global warming of the mantle beneath continents back to the Archaean. Gondwana Res. 15, 254–266. https://doi.org/10.1016/j.gr.2008.10.001.

Correia, P., Murphy, J.B., 2020. Iberian-Appalachian connection is the missing link between Gondwana and Laurasia that confirms a Wegenerian Pangaea configuration. Sci. Rep. 10, 1–7. https://doi.org/10.1038/s41598-020-59461-x.

Dallmeyer, R.D., Wright, J.E., Secor Jr., D.T., Snoke, A.W., 1986. Character of the Alleghanian orogeny in the southern Appalachians: Part II. Geochronological constraints on the tectonothermal evolution of the eastern Piedmont in South Carolina. Geol. Soc. Am. Bull. 97 (11), 1329–1344.

Dallmeyer, R.D., Catalán, J.M., Arenas, R., Ibarguchi, J.G., Gutiérrez, G., Farias, P., Bastida, F., Aller, J., 1997. Diachronous Variscan tectonothermal activity in the NW Iberian Massif: evidence from 40Ar/39Ar dating of regional fabrics. Tectonophysics 277 (4), 307–337.

Daly, L., Pozzi, J.P., 1976. Resultats paleomagnetiques du Permien inferieur et du Trias marocain; comparaison avec les donnees africaines et sud americaines. Earth Planet. Sc. Let. 29 (1), 71–80.

Dang, Z., Zhang, N., Li, Z.-X., Huang, C., Spencer, C.J., Liu, Y., 2020. Weak orogenic lithosphere guides the pattern of plume-triggered supercontinent break-up. Commun. Earth Environ. 1, 1–11. https://doi.org/10.1038/s43247-020-00052-z.

De Boer, J., 1965. Paleomagnetic indications of megatectonic movements in the Tethys. J. Geophys. Res. 70 (4), 931–944.

de Lamotte, D.F., Fourdan, B., Leleu, S., Leparmentier, F., de Clarens, P., 2015. Style of rifting and the stages of Pangea breakup. Tectonics 34, 1009–1029. https://doi.org/10.1002/2014TC003760.

Deenen, M.H.L., Langereis, C.G., van Hinsbergen, D.J.J., Biggin, A.J., 2011. Geomagnetic secular variation and the statistics of palaeomagnetic directions. Geophys. J. Int. 186, 509–520. https://doi.org/10.1111/j.1365-246X.2011.05050.x.

Denyszyn, S.W., Fiorentini, M.L., Maas, R., Dering, G., 2018. A bigger tent for CAMP. Geology 46, 823–826. https://doi.org/10.1130/G45050.1.

Dias da Silva, Í., González Clavijo, E., Díez-Montes, A., 2020. The collapse of the Variscan belt: a Variscan lateral extrusion thin-skinned structure in NW Iberia. Int. Geol. Rev. 00, 1–37. https://doi.org/10.1080/00206814.2020.1719544.

Dias da Silva, Í., González Clavijo, E., Díez-Montes, A., 2021. The collapse of the Variscan belt: a Variscan lateral extrusion thin-skinned structure in NW Iberia. Int. Geol. Rev. 63 (6), 659–695.
Díez Fernández, R., Catalán, J.R.M., Gerdes, A., Abati, J., Arenas, R., Fernández-Suárez, J., 2010. U–Pb ages of detrital zircons from the Basal allochthonous units of NW Iberia: Provenance and paleoposition on the northern margin of Gondwana during the Neoproterozoic and Paleozoic. Gondwana Res. 18 (2–3), 385–399.
Domeier, M., Rob Van der, V., Brett Denny, F, 2011a. Widespread inclination shallowing in Permian and Triassic paleomagnetic data from Laurentia: support from new paleomagnetic data from Middle Permian shallow intrusions in southern Illinois (USA) and virtual geomagnetic pole distributions. Tectonophysics 511 (1-2), 38–52.
Domeier, M., Torsvik, T.H., 2014. Plate tectonics in the late Paleozoic. Geosci. Front. 5, 303–350. https://doi.org/10.1016/j.gsf.2014.01.002.
Domeier, M., Torsvik, T.H., 2019. Full-plate modelling in pre-Jurassic time. Geol. Mag. 156, 261–280. https://doi.org/10.1017/S0016756817001005.
Domeier, M., Van Der Voo, R., Torsvik, T.H., 2012. Paleomagnetism and Pangea: the road to reconciliation. Tectonophysics 514–517, 14–43. https://doi.org/10.1016/j.tecto.2011.10.021.
Domeier, M., Font, E., Youbi, N., Davies, J., Nemkin, S., Van der Voo, R., Perrot, M., Benabbou, M., Boumehdi, M.A., Torsvik, T.H., 2021. On the Early Permian shape of Pangea from paleomagnetism at its core. Gondwana Res. 90, 171–198. https://doi.org/10.1016/j.gr.2020.11.005.
Dominguez, A.R., Van der Voo, R., Torsvik, T.H., Hendriks, B.W., Abrajevitch, A., Domeier, M., Larsen, B.T., Rousse, S., 2011. The≈ 270 Ma palaeolatitude of Baltica and its significance for Pangea models. Geophys. J. Inter. 186 (2), 529–550.
Doucet, L.S., Li, Z.X., El Dien, H.G., Pourteau, A., Murphy, J.B., Collins, W.J., Mattielli, N., Olierook, H.K., Spencer, C.J., Mitchell, R.N., 2020. Distinct formation history for deep-mantle domains reflected in geochemical differences. Nat. Geosci. 13 (7), 511–515.
Edel, J.B., 2001. The rotations of the variscides during the carboniferous collision: Paleomagnetic constraints from the vosges and the massif central (France). Tectonophysics 332, 69–92. https://doi.org/10.1016/S0040-1951(00)00250-X.
Edel, J.B., 2003. Magnetic overprints in granitoids and metamorphic rocks from Limousin (France): evidence for Late Variscan rotations, crustal folding and tilting. Tectonophysics 363, 225–241.
Edel, J.B., Schulmann, K., Lexa, O., Diraison, M., Géraud, Y., 2015. Permian clockwise rotations of the Ebro and Corso-Sardinian blocks during Iberian-Armorican oroclinal bending: preliminary paleomagnetic data from the Catalan Coastal Range (NE Spain). Tectonophysics 657, 172–186. https://doi.org/10.1016/j.tecto.2015.07.002.
Edel, J.B., Schulmann, K., Lexa, O., Lardeaux, J.M., 2018. Late Palaeozoic palaeomagnetic and tectonic constraints for amalgamation of Pangea supercontinent in the European Variscan belt. Earth Sci. Rev. 177, 589–612. https://doi.org/10.1016/j.earscirev.2017.12.007.
Eide, E.A., Torsvik, T.H., 1996. Paleozoic supercontinental assembly, mantle flushing, and genesis of the Kiaman Superchron. Earth Planet. Sci. Let. 144 (3–4), 389–402.
Elmore, R.D., Parnell, J., Engel, M., Woods, S., Abraham, M., Davidson, M., 2000. Paleomagnetic dating of fluid-flow events in dolomitized Caledonian basement rocks, central Scotland. J. Geochem. Explor. 69–70, 369–372. https://doi.org/10.1016/S0375-6742(00)00095-9.
Elmore, R.D., Dulin, S., Engel, M.H., Parnell, J., 2006. Remagnetization and fluid flow in the Old Red Sandstone along the Great Glen Fault, Scotland. J. Geochem. Explor. 89, 96–99. https://doi.org/10.1016/j.gexplo.2005.11.034.
Evans, D.A.D., 2013. Reconstructing pre-Pangean supercontinents. Geol. Soc. Am. Bull. 125, 1735–1751. https://doi.org/10.1130/B30950.1.
Evans, D.A., 2021. Pannotia under prosecution. Geol. Soc. Lond., Spec. Publ. 503 (1), 63–81.
Fossen, H., Ksienzyk, A.K., Rotevatn, A., Bauck, M.S., Wemmer, K., 2021. From widespread faulting to localised rifting: evidence from K-Ar fault gouge dates from the Norwegian North Sea rift shoulder. Basin Res. 33 (3), 1934–1953.
Franke, W., 2000. The mid-European segment of the Variscides: tectonostratigraphic units, terrane boundaries and plate tectonic evolution. In: Orogenic Processes: Quantification and Modelling in the Variscan Belt, pp. 35–61.
Franke, W., Cocks, L.R.M., Torsvik, T.H., 2017. The Palaeozoic Variscan oceans revisited. Gondwana Res. 48, 257–284. https://doi.org/10.1016/j.gr.2017.03.005.
Franke, W., Cocks, L.R.M., Torsvik, T.H., 2020. Detrital zircons and the interpretation of palaeogeography, with the Variscan Orogeny as an example. Geol. Mag. 157 (4), 690–694.
Gaggero, L., Gretter, N., Langone, A., Ronchi, A., 2017. U–Pb geochronology and geochemistry of late Palaeozoic volcanism in Sardinia (southern Variscides). Geosci. Front. 8, 1263–1284. https://doi.org/10.1016/j.gsf.2016.11.015.
Gallo, L.C., Tomezzoli, R.N., Cristallini, E.O., 2017. A pure dipole analysis of the Gondwana apparent polar wander path: Paleogeographic implications in the evolution of Pangea. Geochem. Geophys. Geosyst. 18, 1499–1519. https://doi.org/10.1002/2016GC006692.
Ganbat, A., Tsujimori, T., Miao, L., Safonova, I., Pastor-Galán, D., Anaad, C., Baatar, M., Aoki, S., Aoki, K., Savinskiy, I., 2021. Late Paleozoic–Early Mesozoic granitoids in the Khangay-Khentey basin, Central Mongolia: implication for the tectonic evolution of the Mongol-Okhotsk Ocean margin. Lithos 404, 106455.
Gardiner, N.J., Kirkland, C.L., Van Kranendonk, M.J., 2016. The juvenile hafnium isotope signal as a record of supercontinent cycles. Sci. Rep. 6, 38503. https://doi.org/10.1038/srep38503.
Gurnis, M., 1988. Large-scale mantle convection and the aggregation and dispersal of supercontinents. Nature 332 (6166), 695–699.
Gurnis, M., Yang, T., Cannon, J., Turner, M., Williams, S., Flament, N., Müller, R.D., 2018. Global tectonic reconstructions with continuously deforming and evolving rigid plates. Comput. Geosci. 116, 32–41. https://doi.org/10.1016/j.cageo.2018.04.007.
Gutiérrez-Alonso, G., Fernández-Suárez, J., Weil, Arlo B., 2004. Orocline triggered lithospheric delamination. In: Weil, A.B., Sussman, A. (Eds.), Special Paper 383: Orogenic Curvature: Integrating Paleomagnetic and Structural Analyses. Special Paper. Geological Society of America, Boulder, pp. 121–130. https://doi.org/10.1130/0-8137-2383-3(2004)383[121:OTLD]2.0.CO;2.
Gutiérrez-Alonso, G., Fernández-Suárez, J., Weil, A.B., Brendan Murphy, J., Damian Nance, R., Corfú, F., Johnston, S.T., 2008a. Self-subduction of the Pangaean global plate. Nat. Geosci. 1, 549–553. https://doi.org/10.1038/ngeo250.
Gutiérrez-Alonso, G., Murphy, J.B., Fernández-Suárez, J., Hamilton, M.A., 2008b. Rifting along the northern Gondwana margin and the evolution of the Rheic Ocean: a Devonian age for the El Castillo volcanic rocks (Salamanca, Central Iberian Zone). Tectonophysics 461 (1–4), 157–165.
Gutiérrez-Alonso, G., Fernández-Suárez, J., Jeffries, T.E., Johnston, S.T., Pastor-Galán, D., Murphy, J.B., Franco, M.P., Gonzalo, J.C., 2011a. Diachronous post-orogenic magmatism within a developing orocline in Iberia, European Variscides. Tectonics 30. https://doi.org/10.1029/2010TC002845, 17 PP.-17 PP.
Gutiérrez-Alonso, G., Johnston, S.T., Weil, A.B., Pastor-Galán, D., Fernández-Suárez, J., 2012. Buckling an orogen: The Cantabrian Orocline. GSA Today 22 (7), 4–9.
Gutiérrez-Alonso, G., Collins, A.S., Fernández-Suárez, J., Pastor-Galán, D., González-Clavijo, E., Jourdan, F., Weil, A.B., Johnston, S.T., 2015. Dating of lithospheric buckling:40Ar/39Ar ages of syn-orocline strike-slip shear zones in northwestern Iberia. Tectonophysics 643, 44–54. https://doi.org/10.1016/j.tecto.2014.12.009.
Hatcher, R.D., 2002. Alleghanian (Appalachian) orogeny, a product of zipper tectonics: rotational transpressive continent-continent collision and closing of ancient oceans along irregular margins. Geol. Soc. Am. Spec. Pap. 364, 199–208. https://doi.org/10.1130/0-8137-2364-7.199.
Hatcher, R.D., Tollo, R.P., Bartholomew, M.J., Hibbard, J.P., Karabinos, P.M., 2010. The Appalachian orogen: A brief summary. In: From Rodinia to Pangea: The Lithotectonic Record of the Appalachian Region: Geological Society of America Memoir, 206, pp. 1–19.
Heron, P.J., 2019. Mantle plumes and mantle dynamics in the Wilson cycle. Geol. Soc. Lond., Spec. Publ. 470, 87–103. https://doi.org/10.1144/SP470-2018-97.
Heron, P.J., Lowman, J.P., 2010. Thermal response of the mantle following the formation of a “superplate.”. Geophys. Res. Lett. 37 https://doi.org/10.1029/2010GL045136 n/a–n/a.
Heron, P.J., Murphy, J.B., Nance, R.D., Pysklywec, R.N., 2021. Pannotia’s mantle signature: the quest for supercontinent identification. Geol. Soc. Lond., Spec. Publ. 503 (1), 41–61.
Huebner, Matthew, T., Hatcher, R.D., 2017. "Transition from B-to A-type subduction during closing of the Rheic remnant ocean: New geochronologic and geochemical data marking Acadian-Neoacadian orogenesis and accretion of the Carolina superterrane, southern Appalachians." Linkages and feedbacks in orogenic systems. Geological Society of America Memoir, Philadelphia, pp. 279–312.
Iosifidi, A.G., Mac Niocaill, C., Khramov, A.N., Dekkers, M.J., Popov, V.V., 2010. Palaeogeographic implications of differential inclination shallowing in Permo-Carboniferous sediments from the Donets Basin Ukraine. Tectonophysics 490 (3-4), 229–240.
Irving, E., 1977. Drift of the major continental blocks since the Devonian. Nature 270, 304–309.
Irving, E., 2004. The case for Pangea B, and the intra-Pangean megashear. Geophys. Monogr. 145, 13–27.
Isozaki, Y., Aoki, K., Nakama, T., Yanai, S., 2010. New insight into a subduction-related orogen: a reappraisal of the geotectonic framework and evolution of the Japanese Islands. Gondwana Res. 18, 82–105. https://doi.org/10.1016/j.gr.2010.02.015.
Jacques, D., Muchez, P., Sintubin, M., 2018. Superimposed folding and W-Sn vein-type mineralisation in the Central Iberian Zone associated with late-Variscan oroclinal buckling: a structural analysis from the Regoufe area (Portugal). Tectonophysics 742–743, 66–83. https://doi.org/10.1016/j.tecto.2018.05.021.
Jeleńska, M., Kadzialko-Hofmokl, M., Zelazniewicz, A., 2003. The Devonian - Permian APWP for the west Sudetes Poland. Stud. Geophys. Geod. 47, 419–434. https://doi.org/10.1023/A:1023788127994.
Jesinkey, C., Forsythe, R.D., Mpodozis, C., Davidson, J., 1987. Concordant late Paleozoic paleomagnetizations from the Atacama Desert: implications for tectonic models of the Chilean Andes. Earth Planet. Sc. Let. 85 (4), 461–472.
Jian, P., Liu, D., Sun, X., 2008. SHRIMP dating of the Permo-Carboniferous Jinshajiang ophiolite, southwestern China: geochronological constraints for the evolution of Paleo-Tethys. J. Asian Earth Sci. 32, 371–384. https://doi.org/10.1016/J.JSEAES.2007.11.006.
Johnston, S.T., Gutierrez-Alonso, G., 2010. The North American Cordillera and West European Variscides: contrasting interpretations of similar mountain systems. Gondwana Res. 17 (2–3), 516–525.
K.-Seguin, M., Clark, T., 1985. Reconnaissance paleomagnetic study of igneous rocks from the eastern sector of the Labrador Trough. Can. J. Earth Sci. 22, 1561–1570. https://doi.org/10.1139/e85-165.
Kent, D.V., Muttoni, G., 2020. Pangea B and the Late Paleozoic Ice Age. Palaeogeogr. Palaeoclimatol. Palaeoecol. 553, 109753 https://doi.org/10.1016/j.palaeo.2020.109753.
Kodama, K.P., 2009. Simplification of the anisotropy-based inclination correction technique for magnetite-and haematite-bearing rocks: a case study for the Carboniferous Glenshaw and Mauch Chunk Formations North America. Geophys. J. Inter. 176 (2), 467–477.
Kneller, E.A., Johnson, C.A., Karner, G.D., Einhorn, J., Queffelec, T.A., 2012. Inverse methods for modeling non-rigid plate kinematics: application to mesozoic plate

reconstructions of the Central Atlantic. Comput. Geosci. 49, 217–230. https://doi.org/10.1016/j.cageo.2012.06.019.
Kroner, U., Romer, R.L., 2013. Two plates—many subduction zones: the Variscan orogeny reconsidered. Gondwana Res. 24 (1), 298–329.
Lamotte, F.D., Fourdan, D., Leleu, B., Leparmentier, S., de Clarens, F.P., 2015. Style of rifting and the stages of Pangea breakup. Tectonics 34 (5), 1009–1029.
Lanci, L., Tohver, E., Wilson, A., Flint, S., 2013. Upper Permian magnetic stratigraphy of the lower Beaufort group Karoo basin. Earth Planet. Sci. Let. 375, 123–134.
Leary, R.J., Umhoefer, P., Smith, M.E., Riggs, N., 2017. A three-sided orogen: a new tectonic model for Ancestral Rocky Mountain uplift and basin development. Geology 45, 735–738. https://doi.org/10.1130/G39041.1.
Leite Mendes, B.D., Pastor-Galán, D., Dekkers, M.J., Krijgsman, W., 2021. Avalonia, get bent! – Paleomagnetism from SW Iberia confirms the Greater Cantabrian Orocline. Geosci. Front. 12, 805–825. https://doi.org/10.1016/j.gsf.2020.07.013.
Li, P., Sun, M., Rosenbaum, G., Yuan, C., Safonova, I., Cai, K., Jiang, Y., Zhang, Y., 2018. Geometry, kinematics and tectonic models of the Kazakhstan Orocline, Central Asian Orogenic Belt. J. Asian Earth Sci. 153, 42–56. https://doi.org/10.1016/j.jseaes.2017.07.029.
Liss, D., Owens, W.H., Hutton, D.H.W., 2004. New palaeomagnetic results from the Whin Sill complex: evidence for a multiple intrusion event and revised virtual geomagnetic poles for the late Carboniferous for the British Isles. J. Geol. Soc. 161, 927–938. https://doi.org/10.1144/0016-764903-156.
Lopez-Carmona, A., Abati, J., Pitra, P., Lee, J.K., 2014. Retrogressed lawsonite blueschists from the NW Iberian Massif: P–T–t constraints from thermodynamic modelling and 40 Ar/39 Ar geochronology. Contrib. Mineral. Petrol. 167 (3), 1–20.
Ma, C., Foster, D.A., Hames, W.E., Mueller, P.A., Steltenpohl, M.G., 2019. From the Alleghanian to the Atlantic: extensional collapse of the southernmost Appalachian orogen. Geology 47, 367–370. https://doi.org/10.1130/G46073.1.
Mac Niocaill, C., 2000. A new Silurian palaeolatitude for eastern Avalonia and evidence for crustal rotations in the Avalonian margin of southwestern Ireland. Geophys. J. Int. 141 (3), 661–671. https://doi.org/10.1046/j.1365-246x.2000.00101.x.
Martínez Catalán, J.R., Arenas, R., Abati, J., Martínez, S.S., García, F.D., Suárez, J.F., Cuadra, P.G., Castiñeiras, P., Barreiro, J.G., Montes, A.D., Clavijo, E.G., Pascual, F.J. R., Andonaegui, P., Jeffries, T.E., Alcock, J.E., Fernández, R.D., Carmona, A.L., 2009. A rootless suture and the loss of the roots of a mountain chain: The Variscan belt of NW Iberia. In: Comptes Rendus Geoscience, Mécanique de l'orogénie varisque: Une vision moderne de le recherche dans le domaine de l'orogénie, 341, pp. 114–126. https://doi.org/10.1016/j.crte.2008.11.004.
Matte, P., 2001. The Variscan collage and orogeny (480-290 Ma) and the tectonic definition of the Armorica microplate: a review. Terra Nova 13, 122–128. https://doi.org/10.1046/j.1365-3121.2001.00327.x.
Meijers, M.J., Hamers, M.F., van Hinsbergen, D.J., van der Meer, D.G., Kitchka, A., Langereis, C.G., Stephenson, R.A., 2010. New late Paleozoic paleopoles from the Donbas Foldbelt (Ukraine): Implications for the Pangea A vs B controversy. Earth Planet. Sci. Let. 297 (1–2), 18–33.
McCabe, C., Channell, J.E.T., 1994. Late Paleozoic remagnetization in limestones of the Craven Basin (northern England) and the rock magnetic fingerprint of remagnetized sedimentary carbonates. J. Geophys. Res. 99, 4603–4612. https://doi.org/10.1029/93JB02802.
McKenzie, D.P., Parker, R.L., 1967. The North Pacific: an example of tectonics on a sphere. Nature 216 (5122), 1276–1280.
McWilliams, C.K., Kunk, M.J., Wintsch, R.P., Bish, D.L., 2013. Determining ages of multiple muscovite-bearing foliations in phyllonites using the 40Ar/39Ar step heating method: applications to the Alleghanian orogeny in central New England. Am. J. Sci. 313 (10), 996–1016.
Merino-Tomé, O.A., Bahamonde, J.R., Colmenero, J.R., Heredia, N., Villa, E., Farias, P., 2009. Emplacement of the Cuera and Picos de Europa imbricate system at the core of the Iberian-Armorican arc (Cantabrian zone, north Spain): new precisions concerning the timing of arc closure. Bull. Geol. Soc. Am. 121, 729–751. https://doi.org/10.1130/B26366.1.
Miller, J.D., Kent, D.V., 1986. Paleomagnetism of the Upper Devonian Catskill Formation from the southern limb of the Pennsylvania Salient: possible evidence of oroclinal rotation. Geophys. Res. Lett. 13, 1173–1176. https://doi.org/10.1029/GL013i011p01173.
Mitchell, R.N., Zhang, N., Salminen, J., Liu, Y., Spencer, C.J., Steinberger, B., Murphy, J. B., Li, Z.X., 2021. The supercontinent cycle. Nat. Rev. Earth Environment 2 (5), 358–374.
Molli, G., Brogi, A., Caggianelli, A., Capezzuoli, E., Liotta, D., Spina, A., Zibra, I., 2020. Late Palaeozoic tectonics in Central Mediterranean: a reappraisal. Swiss J. Geosci. 113 (1), p.1–32.
Moores, E.M., Yikilmaz, M.B., Kellogg, L.H., 2013. Tectonics: 50 years after the revolution. Geol. Soc. Am. Spec. Pap. 500, 321–369.
Müller, R.D., Zahirovic, S., Williams, S.E., Cannon, J., Seton, M., Bower, D.J., Tetley, M. G., Heine, C., Le Breton, E., Liu, S., Russell, S.H.J., Yang, T., Leonard, J., Gurnis, M., 2019. A global plate model including lithospheric deformation along major rifts and orogens since the triassic. Tectonics 38, 1884–1907. https://doi.org/10.1029/2018TC005462.
Murphy, J.B., Nance, R.D., 2008. The Pangea conundrum. Geology 36 (9), 703–706.
Murphy, J.B., Nance, R.D., 2013. Speculations on the mechanisms for the formation and breakup of supercontinents. Geosci. Front. 4, 185–194.
Murphy, J.B., Gutierrez-Alonso, G., Nance, R.D., Fernandez-Suarez, J., Keppie, J.D., Quesada, C., Strachan, R.A., Dostal, J., 2006. Origin of the Rheic Ocean: rifting along a neoproterozoic suture? Geology 34 (5), 325–328.
Murphy, J.B., Braid, J.A., Quesada, C., Dahn, D., Gladney, E., Dupuis, N., 2016. An eastern Mediterranean analogue for the Late Palaeozoic evolution of the Pangaean suture zone in SW Iberia. Geol. Soc. Lond., Spec. Publ. 424 (1), 241–263.
Murphy, J.B., Strachan, R.A., Quesada, C., 2021. Pannotia to Pangaea: Neoproterozoic and Paleozoic Orogenic cycles in the Circum-Atlantic region: a celebration of the career of Damian Nance.
Muttoni, G., Kent, D.V., Garzanti, E., Brack, P., Abrahamsen, N., Gaetani, M., 2003. Early Permian Pangea 'B' to Late Permian Pangea 'A.'. Earth Planet. Sci. Lett. 215, 379–394. https://doi.org/10.1016/S0012-821X(03)00452-7.
Muttoni, G., Gaetani, M., Kent, D.V., Sciunnach, D., Angiolini, L., Berra, F., Garzanti, E., Mattei, M., Zanchi, A., 2009. Opening of the Neo-tethys ocean and the pangea B to pangea A transformation during the permian. GeoArabia 14, 17–48.
Nance, R.D., Worsley, T.R., Moody, J.B., 1988. The supercontinent cycle. Scientific American 259 (1), 72–79.
Nance, R.D., Murphy, J.B., Keppie, J.D., 2002. A Cordilleran model for the evolution of Avalonia. Tectonophysics 352 (1–2), 11–31.
Nance, R.D., Gutiérrez-Alonso, G., Keppie, J.D., Linnemann, U., Murphy, J.B., Quesada, C., Strachan, R.A., Woodcock, N.H., 2010. Evolution of the Rheic Ocean. Gondwana Res. 17, 194–222. https://doi.org/10.1016/j.gr.2009.08.001.
Nance, R.D., Murphy, J.B., Santosh, M., 2014. The supercontinent cycle: a retrospective essay. Gondwana Res. 25, 4–29. https://doi.org/10.1016/j.gr.2012.12.026.
Nawrocki, J., 1993. The Devonian-Carboniferous platform paleomagnetic directions from the Silesian-Cracow arear and their importance for Variscan paleotectonic reconstructions. Geol. Quart. 37, 397–430.
Nawrocki, J., Fanning, M., Lewandowska, A., Polechońska, O., Werner, T., 2008. Palaeomagnetism and the age of the Cracow volcanic rocks (S Poland). Geophys. J. Inter. 174 (2), 475–488.
Niu, Y., 2018. Origin of the LLSVPs at the base of the mantle is a consequence of plate tectonics–a petrological and geochemical perspective. Geosc. Front. 9 (5), 1265–1278.
Ondrejka, M., Li, X.-H., Vojtko, R., Putis, M., Uher, P., Sobocký, T., 2018. Permian A-type rhyolites of the Muráň Nappe, Inner Western Carpathians, Slovakia: in-situ zircon U-Pb SIMS ages and tectonic setting. Geol. Carpath. 69, 187–198. https://doi.org/10.1515/geoca-2018-0011.
Pastor-Galán, D., Gutiérrez-Alonso, G., Zulauf, G., Zanella, F., 2012. Analogue modeling of lithospheric-scale orocline buckling: constraints on the evolution of the Iberian-Armorican arc. Bull. Geol. Soc. Am. 124 https://doi.org/10.1130/B30640.1.
Pastor-Galán, D., Gutiérrez-Alonso, G., Murphy, J.B., Fernández-Suárez, J., Hofmann, M., Linnemann, U., 2013. Provenance analysis of the Paleozoic sequences of the northern Gondwana margin in NW Iberia: passive margin to Variscan collision and orocline development. Gondwana Res. 23 (3), 1089–1103.
Pastor-Galán, D., Martín-Merino, G., Corrochano, D., 2014. Timing and structural evolution in the limb of an orocline: the Pisuerga–Carrión Unit (southern limb of the Cantabrian Orocline, NW Spain). Tectonophysics 622, 110–121.
Pastor-Galán, D., Groenewegen, T., Brouwer, D., Krijgsman, W., Dekkers, M.J., 2015a. One or two oroclines in the Variscan orogen of Iberia? Implications for Pangea amalgamation. Geology 43. https://doi.org/10.1130/G36701.1.
Pastor-Galán, D., Ursem, B., Meere, P.A.A., Langereis, C., 2015b. Extending the Cantabrian Orocline to two continents (from Gondwana to Laurussia). Paleomagnetism from South Ireland. Earth Planet. Sci. Lett. 432 https://doi.org/10.1016/j.epsl.2015.10.019.
Pastor-Galán, D., Dekkers, M.J.M.J., Gutiérrez-Alonso, G., Brouwer, D., Groenewegen, T., Krijgsman, W., Fernández-Lozano, J., Yenes, M., Álvarez-Lobato, F., 2016. Paleomagnetism of the Central Iberian curve's putative hinge: too many oroclines in the Iberian Variscides. Gondwana Res. 39, 96–113. https://doi.org/10.1016/j.gr.2016.06.016.
Pastor-Galán, D., Pueyo, E.L., Diederen, M., García-Lasanta, C., Langereis, C.G., 2018. Late Paleozoic Iberian Orocline(s) and the Missing Shortening in the Core of Pangea. Paleomagnetism From the Iberian Range. Tectonics 37, 3877–3892. https://doi.org/10.1029/2018TC004978.
Pastor-Galán, D., Nance, R.D., Murphy, J.B., Spencer, C.J., 2019. Supercontinents: myths, mysteries, and milestones. Geol. Soc. Lond., Spec. Publ. 470, 39–64. https://doi.org/10.1144/SP470.16.
Pastor-Galán, D., Gutiérrez-Alonso, G., Weil, A.B., 2020. The enigmatic curvature of Central Iberia and its puzzling kinematics. Solid Earth 11, 1247–1273. https://doi.org/10.5194/se-11-1247-2020.
Pereira, M.F., Castro, A., Chichorro, M., Fernández, C., Díaz-Alvarado, J., Martí, J., Rodríguez, C., 2014. Chronological link between deep-seated processes in magma chambers and eruptions: Permo-Carboniferous magmatism in the core of Pangaea (Southern Pyrenees). Gondwana Res. 25, 290–308. https://doi.org/10.1016/J.GR.2013.03.009.
Pereira, M.F., Castro, A., Fernández, C., 2015. The inception of a Paleotethyan magmatic arc in Iberia. In: Geoscience Frontiers, Special Issue: The southern Central Asian Orogenic Belt: Tectonics and Metallogeny, 6, pp. 297–306. https://doi.org/10.1016/j.gsf.2014.02.006.
Pérez-Cáceres, I., Poyatos, D.M., Simancas, J.F., Azor, A., 2017. Testing the Avalonian affinity of the South Portuguese Zone and the Neoproterozoic evolution of SW Iberia through detrital zircon populations. Gondwana Res. 42, 177–192.
Piper, J.D., Crowley, S.F., 1999. Palaeomagnetism of (Palaeozoic) Peel Sandstones and Langness Conglomerate Formation, Isle of Man: implications for the age and regional diagenesis of Manx red beds. Geol. Soc. Lond., Spec. Publ. 160, 213–225. https://doi.org/10.1144/GSL.SP.1999.160.01.15.
Plissart, G., Monnier, C., Diot, H., Mărunţiu, M., Berger, J., Triantafyllou, A., 2017. Petrology, geochemistry and Sm-Nd analyses on the Balkan-Carpathian Ophiolite (BCO–Romania, Serbia, Bulgaria): remnants of a Devonian back-arc basin in the easternmost part of the Variscan domain. J. Geodyn. 105, 27–50.
Pohl, F., Froitzheim, N., Obermüller, G., Tomaschek, F., Schröder, O., Nagel, T.J., Sciunnach, D., Heuser, A., 2018. Kinematics and age of syn-intrusive detachment faulting in the Southern Alps: evidence for Early Permian crustal extension and

implications for the Pangea A versus B controversy. Tectonics 37, 3668–3689. https://doi.org/10.1029/2018TC004974.
Quinn, D., Meere, P.A., Wartho, J.A., 2005. A chronology of foreland deformation: ultra-violet laser Ar-40/Ar-39 dating of syn/late-orogenic intrusions from the Variscides of southwest Ireland. J. Struct. Geol. 27, 1413–1425.
Rapalini, A.E., Vilas, J.F., 1991. Tectonic rotations in the Late Palaeozoic continental margin of southern South America determined and dated by palaeomagnetism. Geophys. J. Inter. 107 (2), 333–351.
Reynolds, R.L., Goldhaber, M.B., Snee, L.W., 1997. Paleomagnetic and 40Ar/39Ar Results from the Grant Intrusive Breccia and Comparison to the Permian Downeys Bluff Sill–evidence for Permian Igneous Activity at Hicks Dome Southern Illinois Basin (No. 2094). US Government Printing Office.
Robert, B., Domeier, M., Jakob, J., 2021. On the origins of the Iapetus Ocean. Earth Sci. Rev. 221, 103791.
Rolf, T., Coltice, N., Tackley, P.J., 2012. Linking continental drift, plate tectonics and the thermal state of the Earth's mantle. Earth Planet. Sci. Lett. 351, 134–146.
Rolland, Y., 2017. Caucasus collisional history: review of data from East Anatolia to West Iran. Gondwana Res. 49, 130–146. https://doi.org/10.1016/j.gr.2017.05.005.
Rolland, Y., Hässig, M., Bosch, D., Meijers, M.J.M., Sosson, M., Bruguier, O., Adamia, Sh., Sadradze, N., 2016. A review of the plate convergence history of the East Anatolia-Transcaucasus region during the Variscan: insights from the Georgian basement and its connection to the Eastern Pontides. J. Geodyn. Subduction Orogeny 96, 131–145. https://doi.org/10.1016/j.jog.2016.03.003.
Safonova, I.Y., Santosh, M., 2014. Accretionary complexes in the Asia-Pacific region: tracing archives of ocean plate stratigraphy and tracking mantle plumes. Gondwana Res. 25 (1), 126–158.
Sánchez-Navas, A., García-Casco, A., Mazzoli, S., Martín-Algarra, A., 2017. Polymetamorphism in the Alpujarride Complex, Betic Cordillera South Spain. The J. Geol. 125 (6), 637–657.
Sandoval, L., Welford, J.K., MacMahon, H., Peace, A.L., 2019. Determining continuous basins across conjugate margins: the East Orphan, Porcupine, and Galicia Interior basins of the southern North Atlantic Ocean. Mar. Pet. Geol. 110, 138–161. https://doi.org/10.1016/j.marpetgeo.2019.06.047.
Scotese, C.R., Song, H., Mills, B.J., van der Meer, D.G., 2021. Phanerozoic paleotemperatures: The earth's changing climate during the last 540 million years. Earth Sci. Rev. 103503.
Setiabudidaya, D., Piper, J.D.A., Shaw, J., 1994. Palaeomagnetism of the (Early Devonian) Lower Old Red Sandstones of South Wales: implications to Variscan overprinting and differential regional rotations, 231, 257–280.
Shafaii Moghadam, H., Stern, R.J., 2014. Ophiolites of Iran: keys to understanding the tectonic evolution of SW Asia: (I) Paleozoic ophiolites. J. Asian Earth Sci. 91, 19–38. https://doi.org/10.1016/j.jseaes.2014.04.008.
Shaw, J., Johnston, S.T., Gutiérrez-Alonso, G., 2015. Orocline formation at the core of Pangea: a structural study of the Cantabrian orocline, NW Iberian Massif. Lithosphere 7 (6), 653–661.
Smethurst, M., Briden, J., 1988. Palaeomagnetism of Silurian sediments in W Ireland: evidence for block rotation in the Caledonides. Geophys. J. Int. 95, 327–346.
Smethurst, M.A., Mac Niocaill, C., Ryan, P.D., 1994. Oroclinal bending in The Caledonides of Western Ireland. J. Geol. Soc. 151, 315–328. https://doi.org/10.1144/Gsjgs.151.2.0315.
Speight, J.M., Mitchell, J.G., 1979. The Permo-Carboniferous dyke-swarm of northern Argyll and its bearing on dextral displacement on the Great Glen Fault. J. Geol. Soc. 136 (1), 3–11.
Spencer, C.J., Hawkesworth, C., Cawood, P., Dhuime, B., Spencer, C.J., Hawkesworth, C., Cawood, P., Dhuime, B., 2013. Not all supercontinents are created equal: Gondwana-Rodinia case study. Geology 41, 795–798. https://doi.org/10.1130/G34520.1.
Stampfli, G.M., Borel, G.D., 2002. A plate tectonic model for the Paleozoic and Mesozoic constrained by dynamic plate boundaries and restored synthetic oceanic isochrons. Earth Planet. Sci. Lett. 196 (1–2), 17–33.
Stampfli, G.M., Hochard, C., Vérard, C., Wilhem, C., VonRaumer, J., 2013. The formation of Pangea. Tectonophysics 593, 1–19. https://doi.org/10.1016/j.tecto.2013.02.037.
Steinberger, B., Torsvik, T.H., 2008. Absolute plate motions and true polar wander in the absence of hotspot tracks. Nature 452, 620–623. https://doi.org/10.1038/nature06824.
Storetvedt, K.M., Tveit, E., Deutsch, E.R., Murthy, G.S., 1990. Multicomponent magnetizations in the Foyers Old Red Sandstone (northern Scotland) and their bearing on lateral displacements along the Great Glen Fault. Geophys. J. Int. 102, 151–163. https://doi.org/10.1111/j.1365-246X.1990.tb00537.x.
Storetvedt, K.M., Murthy, G.S., Deutsch, E.R., 1993. Magnetization history of the Upper Silurian Dingle Group, SW Ireland. Geophys. J. Int. 114, 687–695. https://doi.org/10.1111/j.1365-246X.1993.tb06997.x.
Talavera-Mendoza, O., Ruiz, J., Gehrels, G.E., Meza-Figueroa, D.M., Vega-Granillo, R., Campa-Uranga, M.F., 2005. U–Pb geochronology of the Acatlán Complex and implications for the Paleozoic paleogeography and tectonic evolution of southern Mexico. Earth Planet. Sci. Let. 235 (3–4), 682–699.
Thompson, R., Mitchell, J.G., 1972. Palaeomagnetic and radiometric evidence for the age of the lower boundary of the Kiaman magnetic interval in South America. Geophys. J. Inter. 27 (2), 207–214.
Tait, J., Bachtadse, V., Franke, W., Soffel, H.C., 1997. Geodynamic evolution of the European Variscan fold belt: palaeomagnetic and geological constraints. Geol. Rundsch. 86, 585. https://doi.org/10.1007/s005310050165.
Torsvik, T.H., Steinberger, B., Cocks, L.R.M., Burke, K., 2008. Longitude: linking Earth's ancient surface to its deep interior. Earth Planet. Sci. Let. 276 (3–4), 273–282.
Torsvik, T.H., Cocks, L.R.M., 2017. Earth History and Palaeogeography.
Torsvik, T.H., Trench, A., Svensson, I., Walderhaug, H.J., 1993. Palaeogeographic Significance of Mid-Silurian Palaeomagnetic Results from Southern Britain-Major Revision of the Apparent Polar Wander Path for Eastern Avalonia, pp. 651–668.
Torsvik, Trond H., Voo, R.V.D., Preeden, U., Mac, C., Steinberger, B., Doubrovine, P.V., Hinsbergen, D.J.J.V., Domeier, M., Gaina, C., Tohver, E., Meert, J.G., Mccausland, P. J., Cocks, L.R.M., 2012. Phanerozoic polar wander, palaeogeography and dynamics. Earth Sci. Rev. 114, 325–368. https://doi.org/10.1016/j.earscirev.2012.06.007.
Tsujimori, T., Ernst, W.G., 2014. Lawsonite blueschists and lawsonite eclogites as proxies for palaeo-subduction zone processes: a review. J. Metamorph. Geol. 32, 437–454. https://doi.org/10.1111/jmg.12057.
Turrillot, P., Augier, R., Monié, P., Faure, M., 2011. Late orogenic exhumation of the Variscan high-grade units (South Armorican Domain, western France), combined structural and 40Ar/39Ar constraints. Tectonics 30. https://doi.org/10.1029/2010TC002788, 27 PP.-27 PP.
Vacek, F., Žák, J., 2019. A lifetime of the Variscan orogenic plateau from uplift to collapse as recorded by the Prague Basin, Bohemian Massif. Geol. Mag. 156 (3), 485–509.
van der Voo, R., 1993. Paleomagnetism of the Atlantic, Tethys and Iapetus Oceans. Cambridge University Press.
van der Voo, R., Stamatakos, J.A., Pares, J.M., 1997. Kinematic constraints on thrust-belt curvature from syndeformational magnetizations in the Lagos del Valle Syncline in the Cantabrian Arc, Spain. J. Geophys. Res. Solid Earth 102, 10105–10119.
Van Hilten, D., 1964. Evaluation of some geotectonic hypotheses by paleomagnetism. Tectonophysics 1 (1), 3–71.
van Hinsbergen, D.J.J., Torsvik, T.H., Schmid, S.M., Maţenco, L.C., Maffione, M., Vissers, R.L.M., Gürer, D., Spakman, W., 2020. Orogenic architecture of the Mediterranean region and kinematic reconstruction of its tectonic evolution since the Triassic. Gondwana Res. 81, 79–229. https://doi.org/10.1016/j.gr.2019.07.009.
Van Staal, C.R., Dewey, J.F., Mac Niocaill, C., McKerrow, W.S., 1998. The Cambrian-Silurian tectonic evolution of the northern Appalachians and British Caledonides: history of a complex, west and southwest Pacific-type segment of Iapetus. Geol. Soc. Lond., Spec. Publ. 143 (1), 197–242.
van Staal, C.R., Whalen, J.B., Valverde-Vaquero, P., Zagorevski, A., Rogers, N., 2009. Pre-Carboniferous, episodic accretion-related, orogenesis along the Laurentian margin of the northern Appalachians. Geol. Soc. Lond., Spec. Publ. 327 (1), 271–316.
Vine, F.J., Matthews, D.H., 1963. Magnetic anomalies over oceanic ridges. Nature 199 (4897), 947–949.
Waldron, J.W., Schofield, D.I., Murphy, J.B., Thomas, C.W., 2014. How was the Iapetus Ocean infected with subduction? Geology 42 (12), 1095–1098.
Waldron, J.W., Barr, S.M., Park, A.F., White, C.E., Hibbard, J., 2015. Late Paleozoic strike-slip faults in Maritime Canada and their role in the reconfiguration of the northern Appalachian orogen. Tectonics 34 (8), 1661–1684.
Wang, C., Mitchell, R.N., Murphy, J.B., Peng, P., Spencer, C.J., 2020. The role of megacontinents in the supercontinent cycle. Geology. https://doi.org/10.1130/G47988.1.
Warsame, H.S., McCausland, P.J., White, C.E., Barr, S.M., Dunning, G.R., Waldron, J.W., 2021. Meguma terrane orocline: U–Pb age and paleomagnetism of the Silurian Mavillette gabbro, Nova Scotia, Canada. Can. J. Earth Sci. 58 (4), 315–331.
Weil, A.B., van der Voo, Rob, Van Der Pluijm, B.A., 2001. Oroclinal Bending and Evidence Against the Pangea Megashear: The Cantabria-Asturias Arc (Northern Spain). Geology 29 (11), 991–994.
Weil, A.B., Van Voo, R., Der, Pluijm, Van Der, B.A., Pare, J.M., 2000. The Formation of an Orocline by Multiphase Deformation: A Paleomagnetic Investigation of the Cantabria ± Asturias Arc (Northern Spain), p. 22.
Weil, A.B., Gutiérrez-Alonso, G., Conan, J., 2010. New time constraints on lithospheric-scale oroclinal bending of the Ibero-Armorican Arc: a palaeomagnetic study of earliest Permian rocks from Iberia. J. Geol. Soc. 167, 127–143. https://doi.org/10.1144/0016-76492009-002.
Weil, Arlo B., Gutiérrez-Alonso, G., Johnston, S.T., Pastor-Galán, D., 2013. Kinematic constraints on buckling a lithospheric-scale orocline along the northern margin of Gondwana: A geologic synthesis. Tectonophysics 582, 25–49. https://doi.org/10.1016/j.tecto.2012.10.006.
Wesphal, M., Montigny, R., Thuizat, R., Bardon, C., Bossert, A., Hamzeh, R., Rolley, J.P., 1979. Paléomagnétisme et datation du volcanisme permien, triasique et crétacé du Maroc. Canadian J. Earth Sci. 16 (11), 2150–2164.
Wilson, J.T., 1966. Did the Atlantic Close and then Re-Open? Nature 211 (5050), 676–681.
Wilson, B.M., Neumann, E.R., Davies, G.R., Timmerman, M.J., Heeremans, M., Larsen, B. T., 2004. Permo-carboniferous magmatism and rifting in Europe. Geol. Soc. 223 (1), 1–10.
Worsley, T.R., Nance, R.D., Moody, J.B., 1986. Tectonic cycles and the history of the Earth's biogeochemical and paleoceanographic record. Paleoceanography 1 (3), 233–263.
Wu, L., Murphy, J.B., Quesada, C., Li, Z.-X., Waldron, J.W.F., Williams, S., Pisarevsky, S., Collins, W.J., 2021. The amalgamation of Pangea: Paleomagnetic and geological observations revisited. GSA Bull. 133 (3-4).
Xiao, W.J., Windley, B.F., Sun, S., Li, J.L., Huang, B.C., Han, C.M., et al., 2015. A tale of amalgamation of three Permo-Triassic collage systems in Central Asia: Oroclines, sutures, and terminal accretion. Annu. Rev. Earth Planet. Sci. 43, 477–507.
Yeh, M.-W., Shellnutt, J.G., 2016. The initial break-up of Pangæa elicited by Late Palæozoic deglaciation. Sci. Rep. 6, 1–9. https://doi.org/10.1038/srep31442.
Yoshida, M., Hamano, Y., 2015. Pangea breakup and northward drift of numerical model of mantle convection. Sci. Rep. 5, 8407. https://doi.org/10.1038/srep08407.
Yoshida, M., Santosh, M., 2011. Supercontinents, mantle dynamics and plate tectonics: A perspective based on conceptual vs. numerical models. Earth Sci. Rev. 105, 1–24.

Yuan, K., Van der Voo, R., Bazhenov, M.L., Bakhmutov, V., Alekhin, V., Hendriks, B.W. H., 2011. Permian and Triassic palaeolatitudes of the Ukrainian shield with implications for Pangea reconstructions. Geophys. J. Inter. 184 (2), 595–610.

Yuan, S., Neubauer, F., Liu, Y., Genser, J., Liu, B., Yu, S., Chang, R., Guan, Q., 2020. Widespread Permian granite magmatism in Lower Austroalpine units: significance for Permian rifting in the Eastern Alps. Swiss J. Geosci. 113, 18. https://doi.org/10.1186/s00015-020-00371-5.

Zegers, T.E., Dekkers, M.J., Bailly, S., 2003. Late Carboniferous to Permian remagnetization of Devonian limestones in the Ardennes: role of temperature, fluids, and deformation. J. Geophys. Res. Solid Earth 108. https://doi.org/10.1029/2002JB002213 n/a–n/a.

Zeh, A., Hansch, R., Bratz, H., Bombach, K., 2000. Provenance and alteration of granite gravels in Rotliegend beds from the northwestern Thuringian Forest: Results of petrography, geochemistry and zircon investigations. Neues Jahrbuch Fur Geologie Und Palaontologie-Abhandlungen 218, 173–199.

Zhang, X.-Z., Dong, Y.-S., Wang, Q., Dan, W., Zhang, C., Deng, M.-R., Xu, W., Xia, X.-P., Zeng, J.-P., Liang, H., 2016. Carboniferous and Permian evolutionary records for the Paleo-Tethys Ocean constrained by newly discovered Xiangtaohu ophiolites from central Qiangtang, central Tibet. Tectonics 35, 1670–1686. https://doi.org/10.1002/2016TC004170.

Zi, J.-W., Cawood, P.A., Fan, W.-M., Wang, Y.-J., Tohver, E., 2012. Contrasting rift and subduction-related plagiogranites in the Jinshajiang ophiolitic mélange, southwest China, and implications for the Paleo-Tethys. Tectonics 31. https://doi.org/10.1029/2011TC002937.

Ziegler, P.A., 1990. Collision related intra-plate compression deformations in western and central-Europe. J. Geodyn. 11, 357–388.

Ziegler, P.A., 1992. Plate tectonics, plate moving mechanisms and rifting. Tectonophysics 215 (1–2), 9–34.